DEVELOPMENT OF AG ENHANCED TEXTURED POWDER BI-2212/AG SUPERCONDUCTING WIRE TECHNOLOGY

A Dissertation

by

JOSHUA NORMAN KELLAMS

Submitted to the Office of Graduate and Professional Studies of
Texas A&M University
in partial fulfillment of the requirements for the degree of

DOCTOR OF PHILOSOPHY

Chair of Committee,	Peter McIntyre
Committee Members,	Artem Abanov
	Bhaskar Dutta
	Alfred McInturff
	Harlan Harris
Head of Department,	Grigory Rogachev

December 2018

Major Subject: Physics

ABSTRACT

The current development technique for Bi-2212 multifilament superconducting wire is the oxide powder in tube process. For this process, phase pure Bi-2212 fine powder is loaded into a silver tube then drawn, stacked, and redrawn until the desired filament size and number is achieved. The wire is then cabled and wound onto its final form where it undergoes a partial melt heat treatment in an overpressure environment of 5 -10 MPa. The entire form is cooled in a controlled way to allow the liquid to recrystallize into phase pure Bi-2212. However, the partial melt heat treatment process leads to several difficulties. Small void spaces within the initial powder can coalesce into large bubbles after the heat treatment. These large bubbles can occlude any supercurrent from traveling along the filament. The melt liquid is also chemically aggressive and will etch and therefore weaken the silver matrix. Lastly, the recrystallized Bi-2212 is not textured and there is limited connectivity between individual crystal formations. Each of these difficulties need to be addressed simultaneously to optimize the performance of future Bi-2212 superconducting wires.

A new method for preparing Bi-2212 multifilament wires is being developed to minimize the effects of the above mentioned difficulties. Fine Bi-2212 powder is homogenously mixed with nano-scale silver powder and uniaxially compressed into square cross section bars. The bars are loaded into a silver tube then drawn, stacked, and redrawn until the desired filament size and number is achieved. To avoid the complications of the partial melt heat treatment a non-melt heat treatment was

developed. The non-melt heat treatment takes advantage of the material properties of the Bi-2212/silver interface. The bulk of the Bi-2212 is never melted, but interconnectivity and grain growth is still achieved.

The cores used to fabricate the multifilament wires display significant superconductivity in liquid nitrogen, but the multifilament wires show no signs of superconductivity. Separate optimization of the wires in liquid helium is required to maximum the supercurrent carrying potential of the multifilament wires. Additional study on oxygen doping during the non-melt heat treatment may also be necessary.

DEDICATION

To my loving parents, Dennis and Robin Kellams. Without your support and guidance throughout my life I would have never made it this far. Thank you for everything.

ACKNOWLEDGEMENTS

I would like to thank my committee members, Dr. Artem Abanov, Dr. Bhaskar Dutta, Dr. Alfred McInturff, and Dr. Harlan Harris, for their guidance and support throughout the course of this research. I would also like to extend a special thanks to my graduate advisor Dr. Peter McIntyre for allowing me space to stumble so that I may learn, while still providing insight whenever I truly needed it. He has shown a shining example of how a scientist should not only care about the work they do, but also about the people they work with.

I am eternally grateful to the team of graduate and undergraduate students that I have worked with during my time working under Dr. McIntyre. The graduate students have provided helpful conversations, inputting new ideas and ways of thinking that helped me overcome hurdles I may have not overcome without them. Several graduate students deserve special recognition for the immense help they have been to me. Kyle Damborsky laid the foundation for this dissertation by pre-texturing Bi-2212 powder using uniaxial force. Nathaniel Pogue played a role as both mentor and friend at the beginning of this project, helping me find a path that lead to what I wanted to accomplish with this work. Others of my fellow students, such as Trey Holik, Elizabeth Sooby, Karie Badgley, Daniel Chavez, Justin Comeaux, Jeff Breightschopff and James Gerity have provided much needed relief, friendship, and mental support that I believe is an absolute requirement to perform a task such as doctoral study. The undergraduates I have had work with me on this project have been an invaluable help. Particularly, Kyle

Shores and Katy O'Quinn who have spent a significant amount of time helping me work toward the completion of this project.

The technical and scientific staff of the group has taught me at least as much as I have learned in the classroom all these years. Ray Garrison has shown me that a CAD drawing is not just simply making a drawing, but is an in-depth and painstaking process. Dr. Dior Sattarov has, with patience and calm, taught me to perform finite element modelling calculations even when my lack of understanding should have elicited aggravation at the very least. Tim Elliott has educated me on more procedures and methods of machining, repair, and general scientific instrument making than I ever imagined I would learn in my lifetime. Dr. Saeed Assadi has shown and explained to me beam dynamics and how it is the reason for all the magnet technology that the group works on.

I would like to thank two people from outside of the group that have been an immense help to this project. John Buttles has provided help and support for anything I have needed with the die assembly used in this project and for that I am extremely grateful. Dr. Lesh Motowidlo provided not only a person I could always contact about any question I had concerning Bi-2212, but also opened his shop to me so that I could spend a week using his tools and expertise to learn how to draw the wire for this project.

My path to Texas A&M University and the completion of this dissertation has been a long road with countless supporters. My undergraduate advisor Dr. Shirvel Stanislaus convinced me to continue my education and go to graduate school. He taught me to think as a scientist, for this and more I am thankful. My master's advisor Dr.

David Grosnick guided me through an analysis using data from Brookhaven's Relativistic Heavy Ion Collider. This in turn led to me to the realization that I found the accelerator hardware more interesting than the data of the experiment. Without Dr. Grosnick I may have never found this field of research that I have enjoyed so much.

CONTRIBUTORS AND FUNDING SOURCES

Contributors

This work was supervised by a dissertation committee consisting of Professors Peter McIntyre, Artem Abanov, Bhaskar Dutta, and Alfred McInturff of the Department of Physics and Professor Harlan Harris of the Department of Electrical and Computer Engineering.

Several tasks described in sections 2, 3, and 4 were performed by undergraduate physics students K. Shores, J. Vandergrifft, and K. O'Quinn under the instruction and supervision of the student (dissertation author). In addition the four point resistance test described in section 2 was performed by a colleague within my advisors group, Nathaniel Pogue

All other work conducted for the dissertation was completed by the student independently.

Funding Sources

There are no outside funding contributions to acknowledge related to the research and compilation of this document.

NOMENCLATURE

HTS	high temperature superconductor
YBCO	yttrium barium copper oxide
BSCCO	bismuth strontium calcium copper oxide
LTS	low temperature superconductor
HEP	high energy physics
NbTi	niobium Titanium
Nb_3Sn	niobium 3 Tin
MgB_2	magnesium di-boride
PIT	powder in tube
CORC®	conductor on round core
OPIT	oxide powder in tube
PM	partial melt
ETP	enhanced textured powder
LN	liquid nitrogen

TABLE OF CONTENTS

LIST OF FIGURES

LIST OF TABLES

Page

1. INTRODUCTION

This introduction is an overview of both the history, and a few basics of superconductivity. It is in no way meant to be a complete treatment of either the historical background, or the physics within it. It is simply meant to pay respect to the pioneering scientists of the field, while introducing some of the necessary concepts and vernacular for understanding this work and why it was performed.

Discovery of Superconductivity

The discovery of superconductivity begins in 1908 at the laboratory of Kammerlingh Onnes located at Leiden University in Netherlands. This is where, for the first time helium was liquefied [1]. Shortly after in 1911 he discovered that the resistance of mercury suddenly disappeared below the temperature of 4.19 K. This marked the first discovery of the phase transition into the superconducting state of materials [2-4]. Onnes continued and found that tin and lead would also transition in a superconducting state at low temperatures [5]. He confirmed that the resistances were not simply below what was measureable at the time but truly zero through persistent current measurements [6-8]. Onnes dreamed that magnetic fields as high as 10 Tesla would be producible with this new discovery. Sadly, due to his own discovery in 1914 of the destructive effects of even small magnetic fields and current limits on the Type I superconductors that he had discovered; that dream would not be realized until much later [9-12].

In 1933 two German physics, Meissner and Oschenfeld, were measuring the magnetic field outside of both lead and tin superconducting samples. They discover that

an applied external field was suddenly expelled from the samples as the sample was cooled below its critical temperature [13]. Now called the Meissner effect, this discovery marked the beginning of superconductivity being considered as a truly different state, rather than simply as perfect conductors. Figure 1 shows how magnetic flux is expelled when the superconducting material is below the critical temperature. Shortly after in 1935 the London brothers Fritz and Heinz proposed a theory to govern the electric and magnetic field in superconductors [14]. The theory explained the Meissner effect by exhibiting an exponential decay of magnetic fields penetrating the superconductor. The depth at which the magnetic field penetrates is called the London

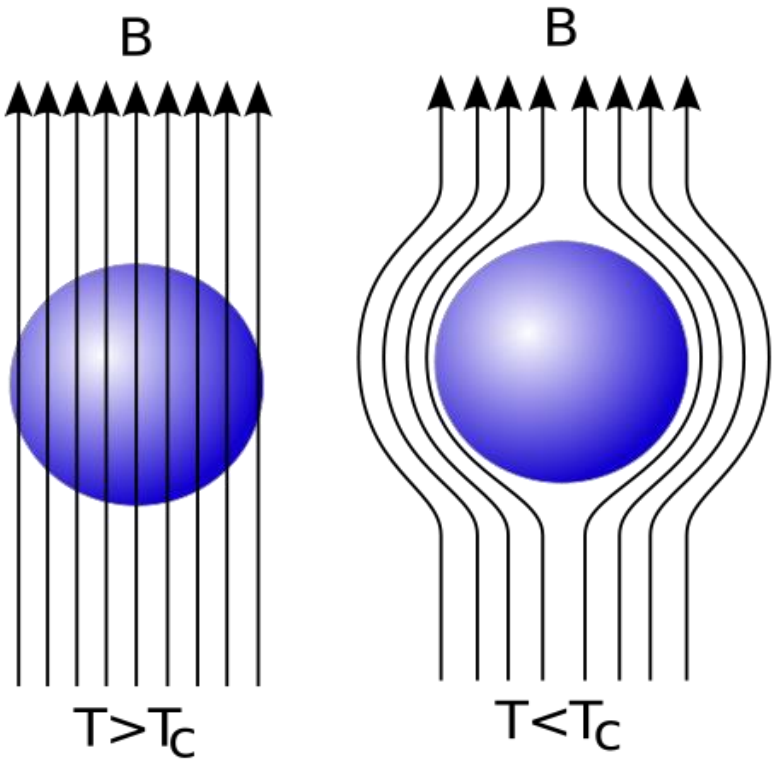

Figure 1: Reprinted from [15]. Diagram showing how the Meissner effect expels flux from a superconducting material when below the critical temperature

penetration depth and is dependent on fundamental constants and the density of superconducting electrons in the given material.

Type II Superconductivity

Shubnikov in 1937, was the first to discover that when certain alloy superconductors are subjected to a magnetic field, the magnetic flux expulsion is not total as it is for type I superconductors, but partial, except for at very low fields [16]. This mixed state, of partially superconducting and partially normal material yields two different critical fields. The first being B_{c1} where the material transitions from completely superconducting to the mixed state, and B_{c2} where the material becomes completely normal. Figure 2 shows a typical B-T plot of a type II superconductor

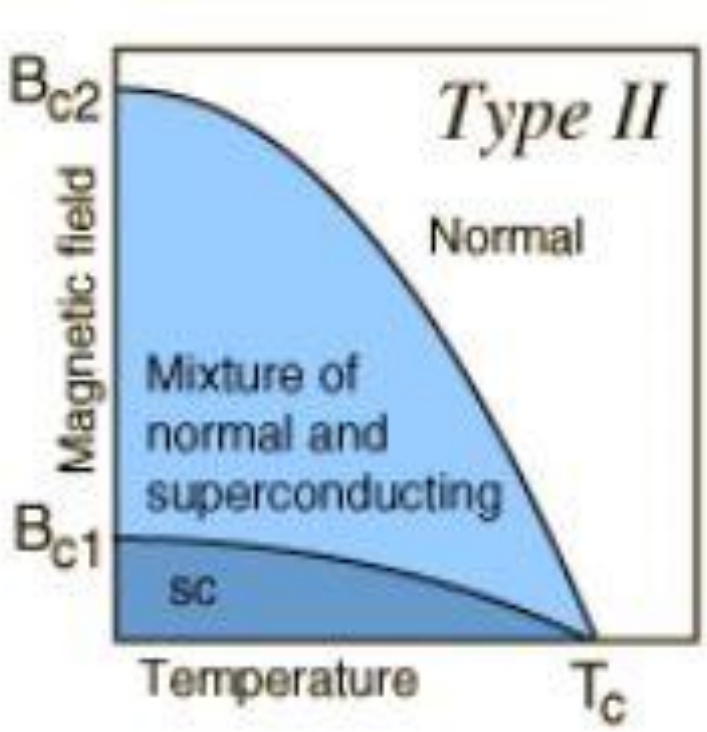

Figure 2: B-T plot of typical type II superconductors showing normal, mixed, and superconducting states.

including the superconducting, mixed, and normal states. This is very important to the practical uses for superconductors since B_{c2} can be much higher than the critical field of Type I superconductors.

Ginzburg and Landau published a famous paper describing a theory of superconductivity in 1950 [17]. This theory made predictions for critical currents in thin superconducting wires and critical fields in thin superconducting films amongst other things. The theory stated that type II superconductors were characterized by negative surface energies between superconducting and normal states and would allow external magnetic fields to permeate the superconductor creating normal regions. The normal regions will be mixed with the superconducting regions in a fine scale so that the boundary surface is maximized. These predictions were in part tested by Zavaritskii in 1952, where it was found that the dependence of critical field on both the thickness of film and temperature did not match Ginzburg and Landau's theory [18]. Abrikosov continued the work of Ginzburg and Landau and amended the theory to fit both the Zavaritskii and type I experimental results, and coined the term type II superconductor [19]. In his theory he described the mixed state of type II superconductors as a vortex state where magnetic vortices penetrated the superconductor and created normal regions instead of what Ginzburg and Landau had theorized, shown in Figure 3. At the lower critical field H_{c1} the vortices begin penetrating the material due to the surface energy between superconducting and normal phases becoming negative. Each magnetic vortex contains a quantized amount of flux ϕ_0. If conditions are stable the vortices form a

lattice as confirmed first by Cribier using neutron diffraction [20, 21] and then again by Trauble and Essman using the decoration method [22].

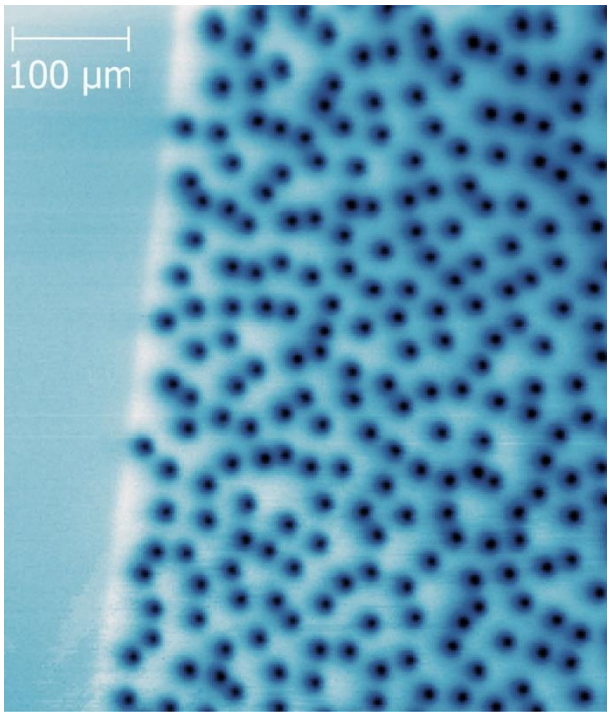

Figure 3: Reprinted from [23]. Vortices shown as black spots on a thin film of Type II superconductor, by means of scanning SQUID microscopy.

The stability of the vortex lattice is the focus of much research when concerning practical uses of superconductors [24]. When the position of a vortex changes energy is dissipated, this is one type of energy release that can cause localized heating or even loss of superconductivity in part of the superconductor. When the superconductor is in a sufficiently large magnetic field the magnetic vortex lattice can "melt" where all vortices are free to move independently and enough energy can be dissipated to cause large areas of superconductor to become normal [25]. The magnetic field at which this happens is called the irreversibility field. Vortices can be held in place using a method called flux

pinning, in which defects or additional grain boundaries are purposely included into the final superconductor to give a position for flux to penetrate [26].

For nearly half a century after the discovery of superconductivity all of the theories had been phenomenological until the triplet of scientists Bardeen, Cooper, and Schrieffer proposed the now famous microscopic theory of superconductivity in 1957 [27]. The theory has been aptly called the BCS theory. The theory verified the phenomenological approaches of the Ginzburg-Landau, and London theories, especially when near the critical temperature. The theory is based around the idea of Cooper pairs, in which two electrons can have a net attractive interaction by exchanging a quasiparticle called a phonon. Phonons are fluctuations in the crystal lattice caused by the presence of an electron traveling through the lattice and creating a vibrational wave. This quasiparticle can cause an attractive interaction between two electrons. If the conditions of the crystal are correct the attractive force due to the phonons can be greater than the repulsive screened Coulomb force, allowing for two electrons to be paired up to a certain distance, called the coherence length.

High Temperature Superconductivity

The focus of this introduction on high temperature superconductivity will be entirely based upon the cuprates, as they are almost exclusively used for applications involving high temperature superconductors (HTS). While other more exotic HTS materials have been discovered and researched, such as the iron-based superconductors and hydrogen sulfide, they have not yet begun the long road of development into practical usage for high field applications [28, 29].

Georg Bednorz and Alex Muller were the first to discover the cuprates (Ba-La-Cu-O) class of superconductor in 1986, achieving a critical temperature of 30 K [30]. Consequently this monumental discovery was immediately recognized and they won a Nobel Prize in Physics the following year. Several months later groups from the Universities of Houston and Alabama jointly discovered yttrium barium copper oxide (YBCO) which had a superconducting transition temperature between 80 K and 93 K [31]. Later the transition temperature was pushed to between 94 K and 98 K as the superconducting phase of YBCO was isolated and tested. The discovery of this high transition temperature material opened the doors of superconductivity in a way that hadn't happened since the initial discovery of superconductivity. Naturally, study continued and it was found that yttrium could be replaced by nearly any rare earth elements and still maintain a transition temperature above 90 K. This class of superconductor is referred to as REBCO. This lead to the belief that superconductivity is confined to copper oxide layer while the rare earth element simply stabilize the structure. As research continued more and more copper oxide compounds were discovered including the focus of this work bismuth strontium calcium copper oxide (BSCCO), which can have a transition temperature of up to 115 K [32]. It is generally accepted that to be called an HTS it must be able to carry supercurrent at liquid nitrogen temperatures (~77 K) as opposed to low temperature superconductors (LTS) that must operate at liquid helium temperature (~4 K). Although not an explicit requirement, HTS superconductors tend to have B_{c2} thresholds > 100 T.

The HTS families of cuprates have very similar crystal structures. They are considered oxygen deficient multi-layered perovskite crystals. Each material contains copper oxide layers in which all superconductivity takes place. However the number of copper oxide layers per crystal cell will differ for each specific material. The number of copper oxide layers per unit cell is related to the critical temperature, shown in Table 1. The general structure of the perovskite crystal causes a large anisotropy in electrical characteristics of the materials in both the normal and superconducting state. Currents flow much easier parallel to the copper oxide layers than they do perpendicular. The structure of bismuth strontium calcium copper oxide will be discussed in more detail in the BSSCO introduction sub-section.

Table 1: Critical temperatures and number of copper oxide layers per crystal cell for several high temperature superconductors.

Formula	Common Name	Tc (K)	# of CuO Layers per unit cell
$YBa_2Cu_3O_7$	YBCO	92	2
$Bi_2Sr_2CuO_6$	Bi-2201	20	1
$Bi_2Sr_2CaCu_2O_8$	Bi-2212	85	2
$Bi_2Sr_2Ca_2Cu_3O_{10}$	Bi-2223	110	3

The mechanism by which superconductivity occurs in cuprates is still being debated. Several theories have been proposed since the discovery of HTS, but none have been verified. A few have developed as favorites, as they can explain some of the behaviors of HTS but none have been experimentally verified completely. A couple of the most popular theories are the weak-coupling theory and interlayer coupling model. The weak coupling theory suggests that HTS behavior is due to antiferromagnetic spin fluctuations. These spin fluctuations act as the quasiparticle called paramagnons that are

analogous to phonons in conventional superconductivity, thereby allowing electron pairs to form. This theory requires that the order parameter from the Ginzburg-Landau theory to have a d-wave symmetry [33]. The second theory is the interlayer coupling model, in which it is suggested that the copper oxide layers can be treated as individual conventional BCS (s-wave) superconductors, but the possibility of tunneling between copper oxide layers allows for an anisotropic s-wave symmetry [34]. Several experiments have been done to test this, and some very compelling evidence has been found suggesting that the pairing symmetry must have a d-wave symmetry with very little s-wave mixing possible [35]. However, other experiments have been performed that suggest mixtures of isotropic s-wave, anisotropic s-wave, and d-wave pairing [35]. To the author's knowledge this symmetry debate has still not reached a conclusion, and even if it does it still does not conclusively give the mechanism by which the electron pairing occurs [36].

Since a theory to explain the microscopic behaviors of HTS does not exist, phenomenological descriptions must be used. A generalized Ginzburg Landau theory is used that includes anisotropic materials [37, 38]. The theory uses an effective mass for each crystal direction resulting in different penetration depths and coherence lengths depending on the anisotropy of the crystal. Another successful theory was developed by treating each copper oxide layer in the HTS as two dimensional, using Ginzburg-Landau theory, and treating all current passing perpendicular to the copper oxide planes as tunneling [39, 40]. This results in coupled Ginzburg Landau equations with a coupling constant as the parameter of the theory. The large success of the theory comes from the

predicted results. If the interlayer coupling is considered weak, the equations yield Josephson current between layers. If the coupling is strong the results are the same as the anisotropic Ginzburg-Landau theory.

The anisotropy of HTS materials affect the way that flux vortices form and behave in the material. A theory was introduced for HTS that the vortices would behave as a "pancake" stack of two dimensional vortices in different layers [41-43], shown in Figure 4. The existence of these vortices were experimentally verified, and showed that they were only weakly coupled to each other and could move out of alignment with each other. HTS vortices can still be pinned, however it is generally much weaker and random if the applied field is parallel to the c axis of the crystal, as in-plane pinning

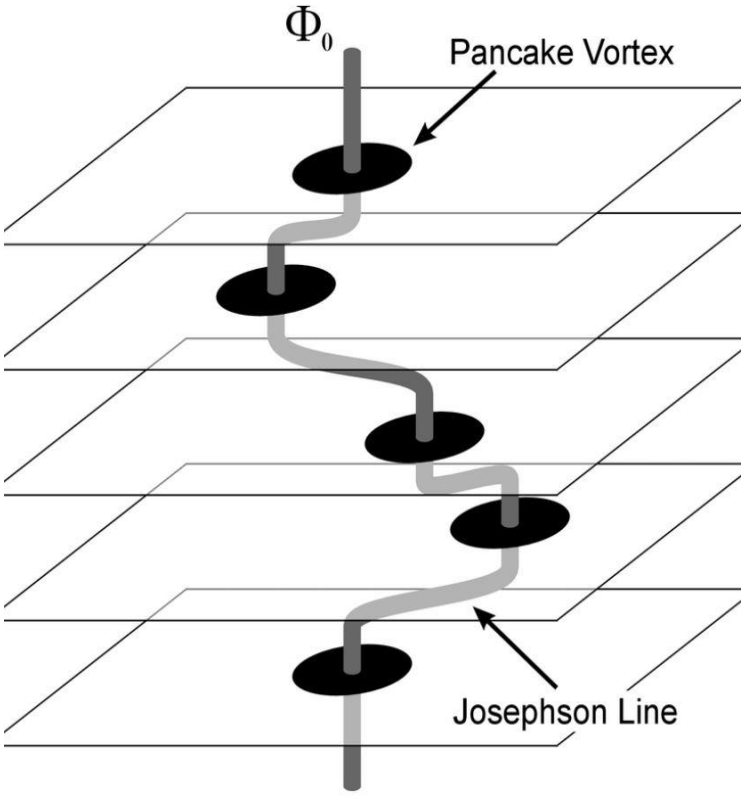

Figure 4: Reprinted from [44]. Graphic displaying pancake vortices and are weakly coupled between each approximately 2-D plain of HTS.

centers are predominately from point defects. Flux pinning can be increased in HTS materials by using grain boundaries as pinning sites or doping the material with artificial pinning centers, making it so that in some cases a less perfect crystal is better for the given application [45]. If the applied field is perpendicular to the c axis increased pinning is observed because the vortex lines can penetrate between copper oxide layers [46].

The behavior of flux vortices in HTS with respect to temperature and external magnetic field can differ drastically when compared to conventional type II superconductors. HTS materials have different phenomenological magnetic field vs temperature (H-T) vortex phases depending on if there are pinning sites or not [24]. Figure 5 shows the phase diagrams with and without pinning sites. If no pinning sites are present the vortex lattice will melt if the field is too high or too low. The case of the vortex lattice melting for a high magnetic field is the same for all type II superconductors, but if the field is too low the shear modulus of the pancake vortices decreases and they are not confined to staying stacked up. If pinning sites are present the phase diagram is even more complicated. The vortex liquid region is now split into pinned and un-pinned liquids with a new phase called vortex glass instead of vortex lattice. The vortex glass region has nearly zero resistivity, and is the truly superconducting state. The pinned liquid region has a resistivity that is less than the normal state resistivity, where the flux vortices are able to flow due to the thermal energy of the system being close to the barrier energy of the pinned vortex state.

Finally, the unpinned liquid has approximately the normal state resistivity where the thermal energy is greater than the barrier energy.

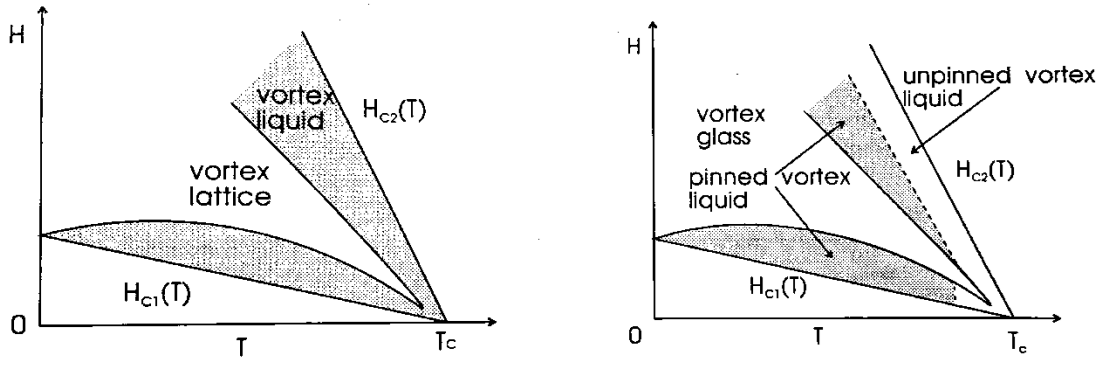

Figure 5: Reprinted from [47]. Typical H-T vortex phases of HTS without (left) and with (right) pinning sites.

Superconductor Applications

The applications for superconductors, particularly type II superconductors, is widespread ranging from the obvious electrical applications, to the more specialized transportation and medical uses. Scientific experiments in nearly every major field of science have adopted superconductor use in their equipment to one end or another. The technology is spreading into commercial products and improving people's daily lives by providing cost savings, convenience, and improved performance.

Electrical applications are the most intuitive uses for superconductors. The use of superconductors in generators reduces both the size and weight of the rotors [48]. This is in addition to the obvious increase in efficiency that zero resistance circuits would cause. LTS material have been used to create superconducting magnetic energy storage machines where in a direct current is applied to the magnet and persistent currents continue with no ohmic losses until the energy is needed and removed. Such

storage could be used for variations in power demand or even energy storage in an emergency situation [49]. Levitating superconductor flywheels with very low friction could be used to store mechanical energy rather than magnetic [50]. Superconducting tapes and wires, particularly HTS, can be used to carry very high current densities for transmission and distribution [51]. This is especially important in urban settings where large power requirements, in relatively small areas, are needed.

The use of superconductors have allowed electromagnets to reach fields that would be impossible by means of resistive electromagnets. This has opened to the doors to both practical advancements and scientific discoveries would have never happened without the discoveries and advancements in the field of superconductivity. High speed magnetically levitating trains, that are safe and environmentally friendly, have been made possible [52]. In addition, the medical field has adopted superconducting magnets in the form of magnetic resonance imaging machines that have helped doctors locate cancers with higher quality images of a person's body than have ever been possible before [53]. The last example that will be given is the main motivation of this work, as it is one of the applications using the largest magnetic fields outside of solenoids. Superconducting particle accelerator magnets have been one of the major limiting factors of high energy physics (HEP) [54]. Modern particle accelerators could not be possible without superconducting dipoles, which allow charged particle beams to be bent along a radius. The magnetic field and radius of the machine is governed by the magnetic rigidity given by:

$$R = B\rho = \frac{p}{q}$$

Where B is the magnetic dipole field, ρ is the radius of the charged particle going through the dipole field, p is the momentum, and q is the charge. It is then plain to see that to increase the energy/momentum of the particle beam either the magnetic field of the bending magnets, radius of the machine, or both must be increased. This has been a major driving force of high current, high field superconductor development. In addition, Superconducting quadrupoles allow beams to be focused and defocused to control the cross sectional size of the particle beam. The list continues with sextupole, octupoles, etc. to control various aspects of particle beams or correct defects of other lower order magnets (dipoles, quadrupoles). Typically these magnetic components have been made of LTS materials but the desire for higher magnetic fields, cost savings, or space savings require the development of HTS materials [55].

Superconducting Materials Used in Scientific Magnets

To justify the purpose of this work, some background on LTS wires and their limitations is needed to understand the need for HTS development. The most common LTS materials that are used in modern particle accelerator are niobium titanium (NbTi), niobium 3 tin (Nb_3Sn), and magnesium diboride (MgB_2). Each of these have gone through their own developments and difficulties, but all three have become stable, reliable, commercially available products.

NbTi was discovered in 1962 at Atomics International by Berlincourt and Hake [56]. It has since become a staple of applied superconductivity due to its high critical current density, affordability, and ability to be relatively easy fabricated into multifilament round wire. Typically rods of NbTi in a copper matrix, are drawn and

restacked until the desired filament size is reached. The multifilament round wire can then be used, or be further processed into Rutherford cable [57]. Figure 6 shows an etched sample of Rutherford cable from the LHC along with a cross sections showing the strands in each wires, and filaments in each strand. Nearly all of the commercially

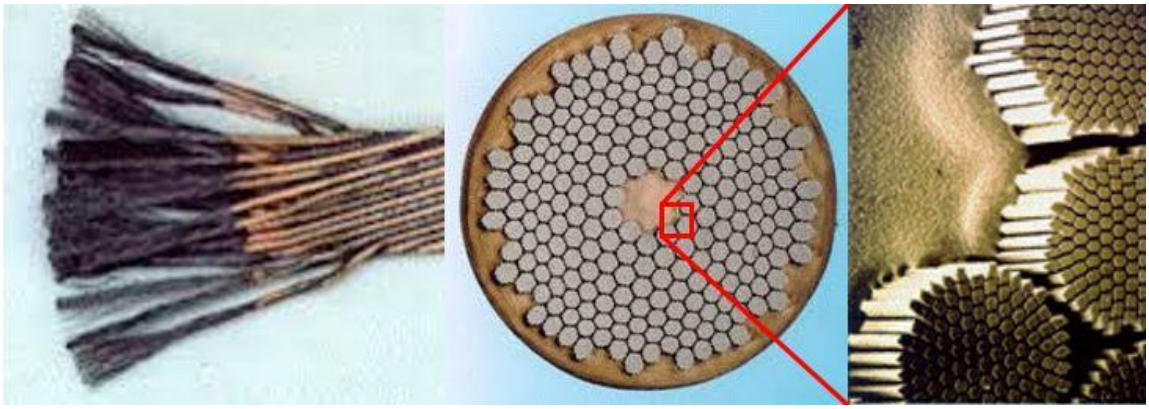

Figure 6: Reprinted from [58]. (Left) Rutherford cable with the copper matrix etched off exposing NbTi filaments. (Middle) Cross section of round wire used in the Rutherford cable showing each strand of filaments. (Right) Micrograph showing filaments within the strand.

available products, consisting mostly of MRI machines, use NbTi. These products require over 3 million kilograms of NbTi to be produced per year making it a ~ 4 billion dollar industry [59]. NbTi has a maximum critical magnetic field of ~ 15 T and a critical temperature of ~ 10 K [60]. It is important to note that while B_{c2} of NbTi is 15 T, that is the magnetic field at which the supercurrent carrying capacity of the material drops to zero and it reverts back to a normal non-superconducting material. Because of this limitation NbTi has historically been used for magnets requiring < 10 T fields. If a magnetic field above 10 T is required the more expensive and more difficult Nb_3Sn is a more appropriate choice of superconductor.

Nb3Sn was discovered in 1954 to be a superconductor [61], but it wasn't until 1961 that its ability to carry high current densities at higher magnetic fields was realized. Nb3Sn has an upper critical field of ~ 30 T allowing it to continue superconducting in fields that are approximately double the maximum of NbTi [62]. It also has a higher critical temperature than NbTi at 18.3 K [63]. Nb3Sn is much more than difficult than NbTi to work with, it is very brittle and is not suitable to wire drawing. To work around this complication precursors are drawn and wound on to the final form and then heat treated to react the niobium and tin to create the Nb3Sn compound. This is typically done by three different methods. The first is the bronze process, in which niobium bars are put into a copper-tin bronze matrix and drawn, stacked, and redrawn [64]. The second method is the internal tin process, in which niobium bars in a copper matrix are drawn and stacked around a large single tin core and redrawn into their final size [65]. Finally a powder-in-tube (PIT) process can be used where all niobium and tin powders are mixed and put in a copper tube to be drawn, stacked and redrawn [66]. Figure 7 shows a diagram of each method. Each of these methods will have different heat treatments, some of which can be quite challenging, but the end goal is the same for each, to have small grain, Nb3Sn, fine filament conductors. A magnetic dipole field of 20 T is technically feasible with a combination of NbTi and Nb3Sn but would be very expensive, a more practical accelerator dipole limit would be 16 T in order to balance cost with performance [67].

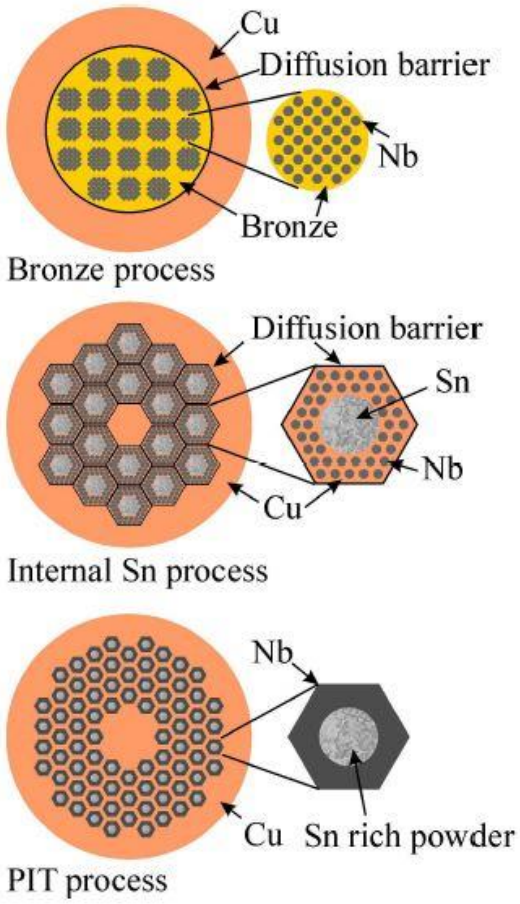

Figure 7: Reprinted from [58]. Diagram showing the basic geometry and configuration of materials for all three main methods of fabricating Nb3Sn wires.

Magnesium diboride was initially synthesized in 1953, but its superconducting properties were not discovered until 2001. It has the highest critical temperature of all the LTS materials at ~ 39 K, making it possible to operate at helium vapor temperatures for cost savings. However the performance is similar to NbTi, so it doesn't contribute much to the development of high field magnets, but it does have a place in the use of lower field applications.

LTS magnets have been all physicists had until the discovery of HTS materials. The HTS materials generally have a high enough critical temperature that they can be operated above 77 K, or liquid nitrogen temperatures. In the case that low current and low magnetic fields are required, liquid nitrogen is significantly cheaper than liquid helium, so HTS may be more economical even if the cost of the conductor is higher. If high current and high field is desired the operating temperature can be dropped down to 4.2 K or lower using liquid helium and HTS can perform in magnetic fields were a LTS material would not superconduct. Significant work has been put into developing these materials to be suitable for the uses in high field magnets and other practical uses. Largely only two families of materials are being developed for such uses, Yttrium barium copper oxide (YBCO) and Bismuth strontium calcium copper oxide (BSCCO).

The first family of HTS, YBCO was discovered in 1986 by Georg Bednorz and Karl Muller at IBM in Zurich, and were awarded the Nobel Prize the following year for being the first to discover an HTS material [30]. The critical temperature of the superconducting phase is 93 K as verified by Wu and Ching-Wu in 1987 [31]. YBCO has experienced limited use in applications, primarily due to the high degree of texture that is necessary, the difficulty of supercurrent passing through grain boundaries, and fabrication difficulties stemming from the brittleness of the material and the powder in tube process not yielding good results. The second family of HTS materials is BSCCO, as it is the material of focus in this work it will have a more detailed introduction section of its own below in the next sub-section.

Due to the brittleness, anisotropic nature, and general low level of workability of HTS material. Two different geometries of practical HTS have been developed, each with pros and cons. The first, tape geometry is where the HTS material is typically grown or deposited onto a metallic tape substrate and layered with stabilizing metal, producing what is essentially a very thin, but wide conductor, shown in Figure 8. These typically have high superconductor to stabilizer ratios and therefore generally have a higher engineering current density than the other geometries. Since HTS materials are generally anisotropic with respect to their crystal structure, the tape geometry maintains a high degree of texture, or alignment of the crystal grains. This leads to low losses due to grain mismatch and a larger degree of control over which direction magnetic flux goes through the superconductor. Tapes can easily be wound on pancake coils, or twisted, but cannot be wound out of plane at all. This places severe

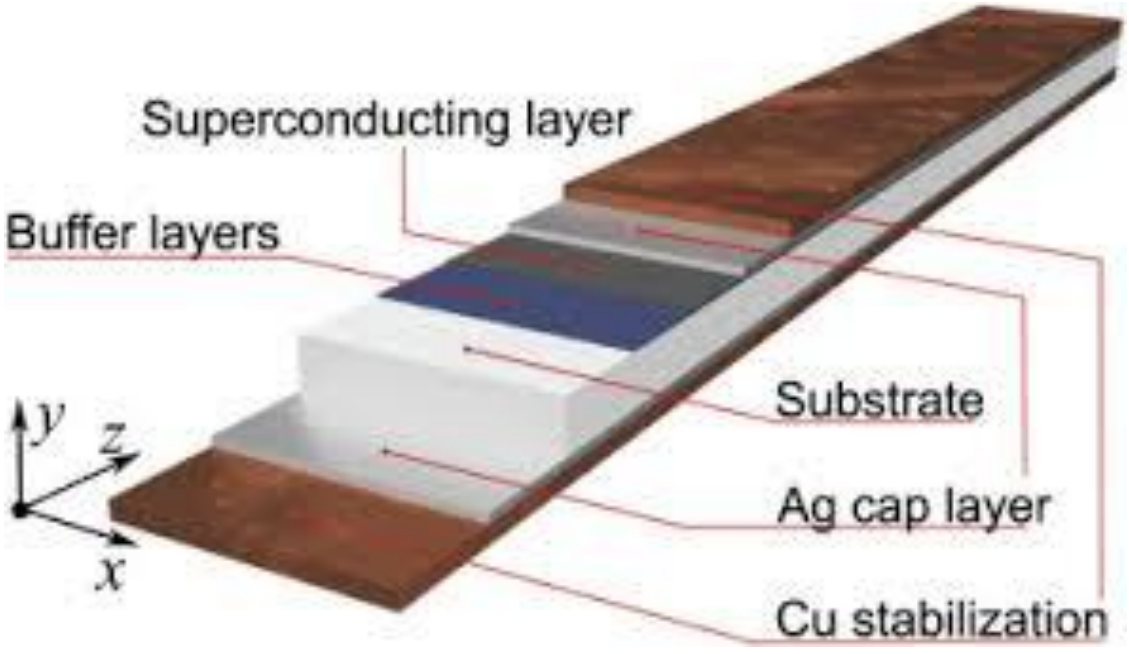

Figure 8: Reprinted from [68]. Configuration of typical HTS tape geometry

limitation on the magnet design that tape can be used for. A method for dealing with this issue has been developed by Advanced Conductor Technologies LLC called conductor on round core (CORC®) cable, in which a REBCO HTS tape is wrapped in a helical fashion onto a core [69]. This allows the tape to be wound in any direction, but the benefits of higher engineering current density and control over magnetic field direction largely disappear. This method was developed as a way to fabricate YBCO into round wire, which is not possible through conventional means. However, the current generation of CORC® cable is only suitable to low inductance application such as fusion and power transmission [70]. The second geometry is multifilament round wire. This method is typically the PIT process described above but using either the HTS precursors, or phase pure ground HTS powder. Typically this method is only used for BSSCO and not YBCO. This process does produce lower ratios of superconductor to matrix, but allows for drastically improved freedom when designing how the wire will be wound onto the final form. This work will be using a variation of the PIT process, where in a compressed bar of BSSCO is inserted into a tube rather than a powder.

BSCCO Introduction

The Bismuth strontium calcium copper oxide (BSCCO) family of superconductors was discovered in 1988 by Maeda [32]. There are several members of the BSCCO family corresponding to different n values of the chemical formula $Bi_2Sr_2Ca_{n-1}Cu_nO_{2n+4+x}$, shown in Table 2. The n = 2 member of the family (Bi-2212) will be the focus of this work, however the other family members of n = 1, 3, and 4 are all superconductors. The n = 1 member (Bi-2201) is of no particular interest as it has a

Table 2: Family of BSCCO superconductors and their feasibility for use in practical superconductors.

$Bi_2Sr_2Ca_{n-1}Cu_nO_{2n+4+x}$			
n	Common Name	T_c (K)	Conductor Feasability
1	Bi-2201	20	No, critical temperature too low
2	Bi-2212	85	Yes
3	Bi-2223	110	Yes, but only in tape form
4	Bi-2234	104	No, difficult to synthesize

considerably lower critical temperature than the others. The n = 3 (Bi-2223) member has been studied significantly with the highest critical temperature of the family, but the atypical distribution of three copper oxide layers in this compound makes it difficult to correctly oxygen dope all layers simultaneously. Finally the n = 4 (Bi-2234) has the second highest critical temperature, but is very difficult to synthesize with the necessary purity due to its location on the phase diagram [71]. In 1991 Bi-2212 had its potential for use in high field magnets with the measurement of the upper critical field B_{c2} = 200+/-25 T at 4.2 K [72]. This coupled with the potential for high irreversibility fields make Bi-2212 a very attractive option for developing applications in high field.

Like all HTS cuprates Bi-2212 has a layered geometry with all superconductivity occurring in the copper oxide planes. There is an oxide of each element except calcium being stacked on top of each other. The calcium layers are situated between the copper oxide layers, shown in Figure 9. This layered geometry causes the material to behave in

a very anisotropic way with respect to the physical, electric and magnetic properties [73]. Some of these anisotropies coupled with the aggressive chemical nature of Bi-2212 have plagued the development of the BSSCO family of superconductor since their discovery.

The anisotropic layered crystal structure of Bi-2212 causes some interesting properties, some of which are hurdles to overcome and others that can be used as a boon to the development. One of these properties is the resistivity of the material. The resistivity of the c axis is significantly higher that the a-b plane [74]. This coupled with the small coherence lengths (ξ_c = 0.4 nm, ξ_{ab} = 3.5 nm), means that the final crystals need to be aligned to a high degree [75]. The reason for this is that BSSCO like all cuprates carry all supercurrent in the CuO_2 layers of the material. The need for a high

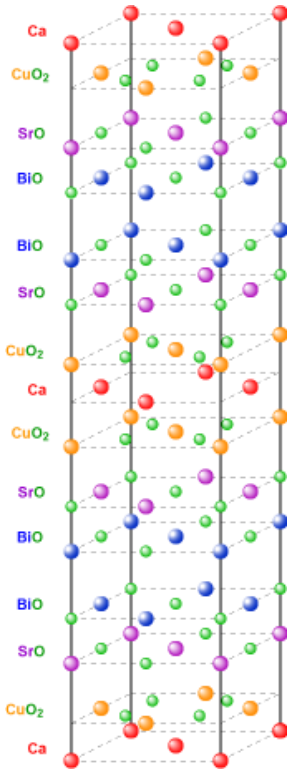

Figure 9: Reprinted from [76]. Layered crystal structure of Bi-2212

degree of crystal grain alignment and interconnectivity causes difficulties for a traditional PIT process. When the liquid is cooled and allowed to recrystallize grains can grow so that the c axis is longitudinal to the wire filament, forcing any current that will flow to travel along the c axis. There is a reasonably strong preference given to crystals with the c axis transverse to the wire filament due to nucleation along the silver/Bi2212 interface, but as the crystal grows into the center of the filament that texture can be lost. This creates mismatches of the grain angles, inter-grain crystal spacing and therefore additional losses in the wire. Figure 10 shows an example filament in which grain misalignment is as high as 20^{o}. Another property is the micaceous nature of the material when ground into a fine powder. The flakes of the powder will easily slide over other particles when they are aligned. The flakes of powder can be aligned when uniaxial force is applied [77]. Traditionally this would be a

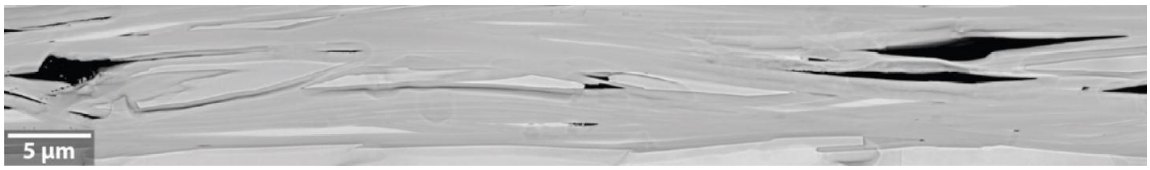

Figure 10: Reprinted from [78]. Bi-2212 filament micrograph showing grain mismatch of +/- 20°

moot step as all memory of any texture is lost when melted, but this work will use this property as a benefit.

Bi-2212 is traditionally used with a silver matrix due to oxygen permeability at high temperatures and it's relatively low cost compared to other oxygen permeable metals. However, Bi-2212 is very chemically aggressive in its liquid form and will etch away the grain boundaries of the silver matrix forming a ~2-5% silver solution with the

liquid Bi-2212 [79]. Traditionally, this has caused difficulties as the heat treatments melts the HTS material, the silver matrix is damaged and will then commonly allow dendritic grows to form between filaments during recrystallization [80, 81]. The filaments can even grow blades that will cut through the matrix entirely and expose the Bi-2212 to the outside environment allowing for carbon, moisture, and other substance that could potentially poison the superconducting properties of the wire [82]. Figure 11

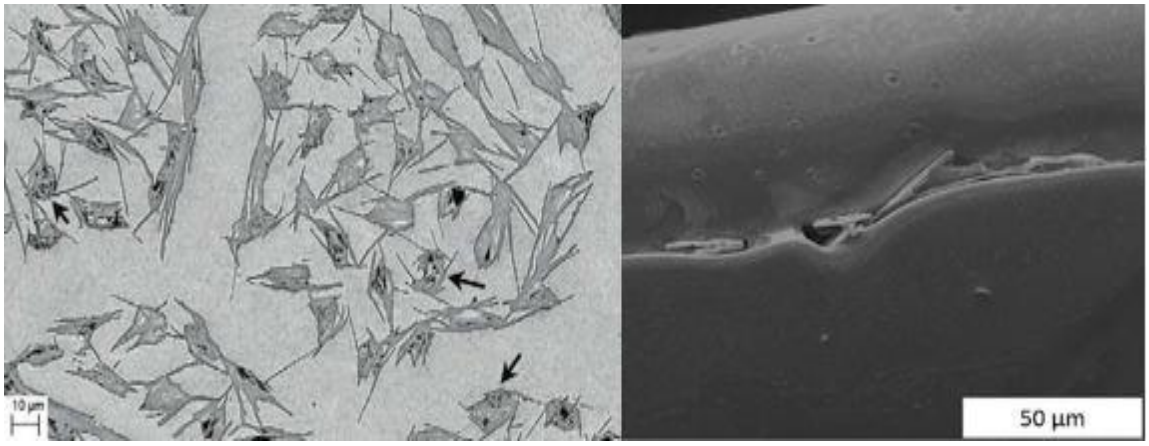

Figure 11: (Left) Reprinted from [83]. Dendritic growths of Bi-2212 between neighboring filaments. (Right) Reprinted from [77]. A blade of Bi-2212 that has grown through the surface of the wire.

shows the dendritic growths connecting each filament to most of its nearest neighboring filaments within the wire, and a blade that has grown through the edge of the wire.

Significant effort has been put in to overcome these hurdles and increase the performance of Bi-2212. To date Bi-2212 remains the only HTS material capable of being fabricated into multifilament round wire, making it arguably the only viable option for the future of high field collider magnets. Current fabrication methods have produced multifilament wires with little to no macroscopic defects, but have yet to produce a process capable of being used on long lengths required for high field collider

magnets. However, small coils have been built, and generated up to 2.6 T in a background field of 31 T [81]

Current Bi-2212 Multifilament Wires

The current state of the art Bi-2212 multifilament wires are made using the oxide powder in tube (OPIT) process. For the OPIT process phase pure Bi-2212 fine powder is loaded into a silver tube and sealed. The tubes are then drawn to densify the powder, stacked, and redrawn, until the desired filament size and number are achieved [84]. The wire can then be cabled into various forms including Rutherford cable [85], and cable in conduit [86, 87]. The cable is then wound onto its final form and undergoes a partial melt (PM) heat treatment. During this heat treatment the Bi-2212 fine powder undergoes a phase transition into a liquid state. It is then allowed to cool in a controlled manner to recrystallize and anneal the Bi-2212. This partial melt process leads to several difficulties:

- The small void spaces that form during loading of the powder can coalesce into larger current occluding bubbles that block filaments when the powder is melted, shown in Figure 12 [81, 88, 89].
- The melt liquid is chemically aggressive and will etch away the silver matrix weakening it [90], making it possible for recrystallization to form dendrites between filaments.

- The recrystallized Bi-2212 from this process is not textured and has limited connectivity between individual crystal formations [81, 91].

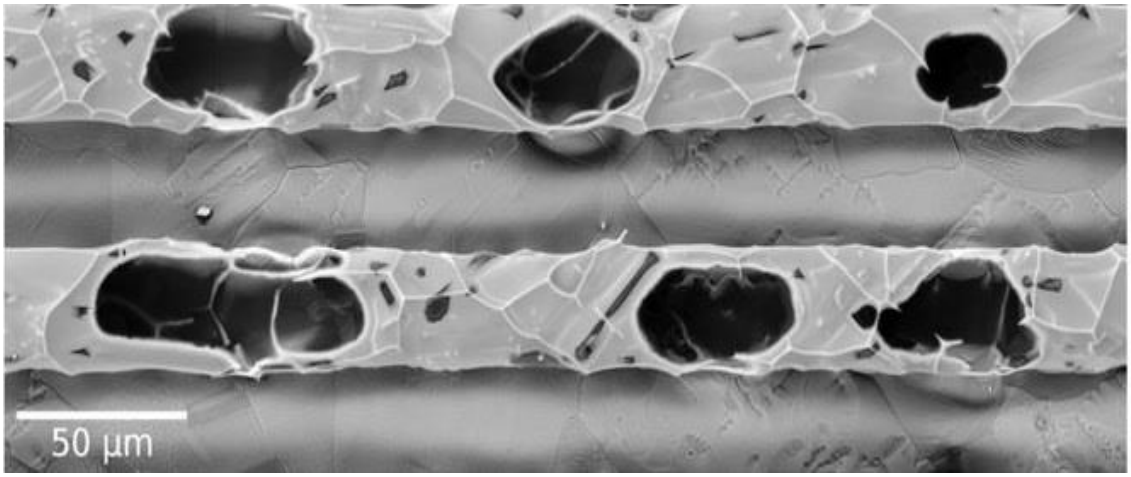

Figure 12: Reprinted from [92]. Large current occluding bubbles within Bi-2212 filaments.

Overpressure process at 5 -10 MPa during the PM heat treatment has made significant improvements to the performance of Bi-2212 wires, by drastically reducing the size of the current occluding bubbles [83, 93-96]. This is done by applying 1 atm partial pressure of oxygen and 49 -99 atm partial pressure of an inert gas, such as nitrogen. The inert gas squeezes the bubbles and keeps them from expanding during the PM heat treatment. This has made great strides in solving the problem of the coalescing bubbles, but has provided no solutions to the problems of matrix etching or texturing of the Bi-2212 during recrystallization. Figure 13 show a comparison between wires with and without over pressure processing, notice the wire burst without over pressuring. Other methods of reducing the bubbles such as densification by groove rolling before heat treatment have made critical current improvement, but not to the performance of overpressure processing [97].

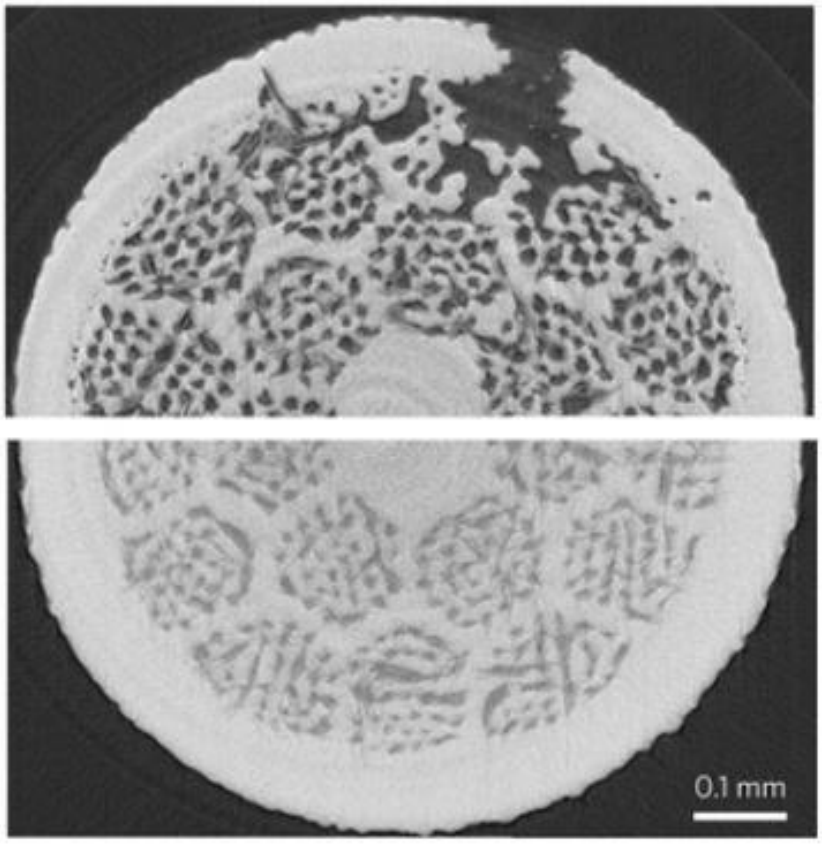

Figure 13: Reprinted from [81]. Multifilament wire heat treated without (top) and with (bottom) over pressure processing.

Textured Powder Development

The groundwork of this dissertation is laid upon the work of a previous graduate student from within Dr. McIntyre's laboratory at Texas A&M University [77]. Dr. Kyle Damborsky developed methods that were instrumental to the completion of this project, and understanding his work is of the utmost importance to understanding the work presented in this dissertation. This section will be devoted to explaining key elements of his work that are essential to understanding this project, the motivations behind it, and will serve as an introduction to some of the methods mentioned above. Following sections will then discuss the improvements and modifications to the methods described

in this section in order to maintain a clear distinction between the work of Dr. Damborsky and the author of this dissertation.

The success of Dr. Damborsky in showing that pure Bi-2212 could be texturized to great than 90% and inserted in a silver tube was influential in the completion of this project. Several methods of pre-texturizing were attempted but it was discovered that large uniaxial pressure (20 KSI) produced the best results. A die set was developed to be used to produce both 4 mm and 1 mm square cross section Bi-2212 rods. Although some of his work is based off of the 1 mm rods they were deemed too fragile and abandoned in favor of the 4 mm variety for the purpose of future work. The same die set was used to create the bars for this project and will be described in section 3, albeit with a substantially modified procedure.

An attempt was made to develop a non-melt heat treatment, but only yielded a Bi-2212 bar that could carry a few amps of supercurrent. However, the microstructure of the bars showed promise, in that the texture was maintained through the heat treatment. It was deemed that the low superconducting properties were likely due to a

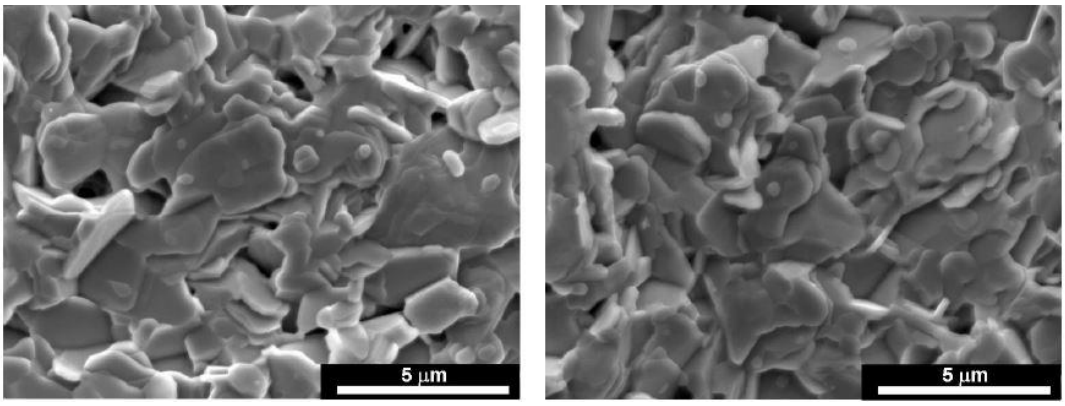

Figure 14: Reprinted from [77]. Micrographs of Bi-2212 pellet produced using Damborsky's method showing large grain growth, but little to no interconnectivity between grains.

lack of connection between Bi-2212 grains. Figure 14 shows a micrograph of a pellet produced and heat treated using Damborsky's methods. It is clearly seen that the grain grown, starting from 1 μm powder, is substantial. It is also easily seen that little to no interconnectivity between grains exists. The results of Damborsky's work inspired and forged a path to the dissertation work being presented in the following sections.

Project Goals and Outline

The goals of this project are to avoid the pitfalls of the OPIT process by developing a new method of fabricating multifilament Bi-2212 wire without the necessity of large scale overpressure processing, while implementing the successes of the textured powder development. Ultimately, either meeting or exceeding the current carrying capacity of the present state the art would be the goal, but that is a monumental undertaking and way beyond the scope of a dissertation for a single graduate student. This project is then divided into four goals.

1. Mix silver nano-scale powder homogenously into micron sized phase pure Bi-2212 to create enhanced powder.
2. Modify the process developed by K. Damborsky to fabricate enhanced textured powder cores with a higher survival rate of the fragile cores.
3. Develop a fabrication method that that can be scaled to create long length multifilament wire using the enhanced textured powder cores
4. Develop a non-melt heat treatment process that will grow and interconnect Bi-2212 grains while maintaining minimum parasitic phases and corrosion of the silver matrix.

While the previous study on texturing yielded positive results for pre-texturing Bi-2212, the attempt at developing a heat treatment showed grain growth but did not show any interconnectivity of those grains. Due to the short coherence length of Bi-2212 the grains need to be connected intimately to allow supercurrent transport. This work will show that by introducing an enhancement of silver nano-powder and developing a non-melt heat treatment, interconnectivity can be achieved while still maintaining the pre-texturing of the Bi-2212. In addition this work will further develop the process of producing pre-textured Bi-2212 cores and using them to be able to draw long lengths of superconducting wire. The process of drawing the wire was also simplified drastically, and by simplifying the process the superconducting core maintained its original square cross rather than being deformed.

2. ENHANCED TEXTURED POWDER*

The results of the textured powder study described in section 1 dictated that while Bi-2212 is capable of being pre-textured before heat treatment, an enhancement of the powder would be necessary to yield connected grains while maintaining a non-melt heat treatment. The enhanced textured powder (ETP) comes in the form of silver nano-powder being homogenously mixed into the Bi-2212 before any other processing is done. In order to homogenously mix the silver nano-powder with the Bi-2212 fine powder a high acceleration mixing was necessary. The silver nano-powder tends to form aggregates that need to be broken during mixing. Figure 15 shows the homogenous mixtures of both the 20 nm and 100 nm silver powders. Studies have been published on adding various metal powders to Bi-2212 including silver [98-100], but to

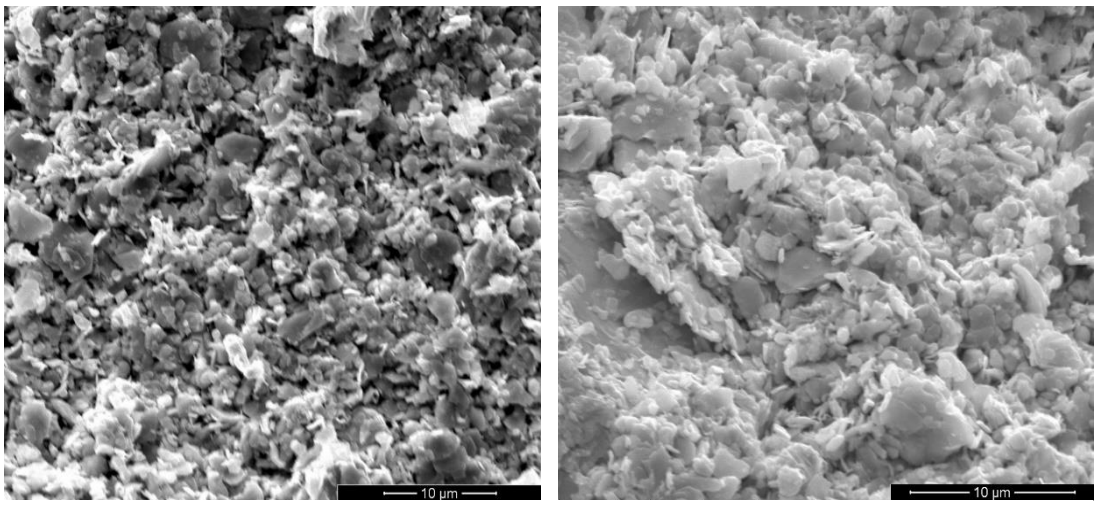

Figure 15: Homogenous mixtures of Bi-2212 fine powder and silver nano-powder of average sizes 20 nm (left) and 100 nm (right). The silver particles are the small objects interspersed between the 1 µm Bi-2212 particles.

*Part of the data reported in this section is reprinted from J. Kellams *et al* Presented at the 2015 IPAC, Richmond VA, USA [101]

*Part of the data reported in this section is reprinted from J N Kellams *et al* Presented at the 2015 CEC-ICMC, Tucson AZ, USA [102]

the knowledge of the author this is the first study that has been performed to advantageously use the well-known property that the melt temperature of Bi-2212 decreases slightly at the Bi-2212 interface [79]. Nano-powder was chosen to maximize the surface contact with the Bi-2212 grains while minimizing the amount of silver. This addition of silver powder also mitigates the corrosive effect that Bi-2212 has on the silver matrix during heat treatment [90].

A sample of the enhanced powder needed to be pressed to verify that the addition of the silver nano-powder did not interfere with the Bi-2212 powder's ability to hold its final pressed form or drastically affect the pre-texture. A sample of enhanced powder was pressed at 20 KSI to repeat the optimal pressure from K. Damborsky's study. A small pellet geometry was chosen to limit the amount of enhanced powder that was used.

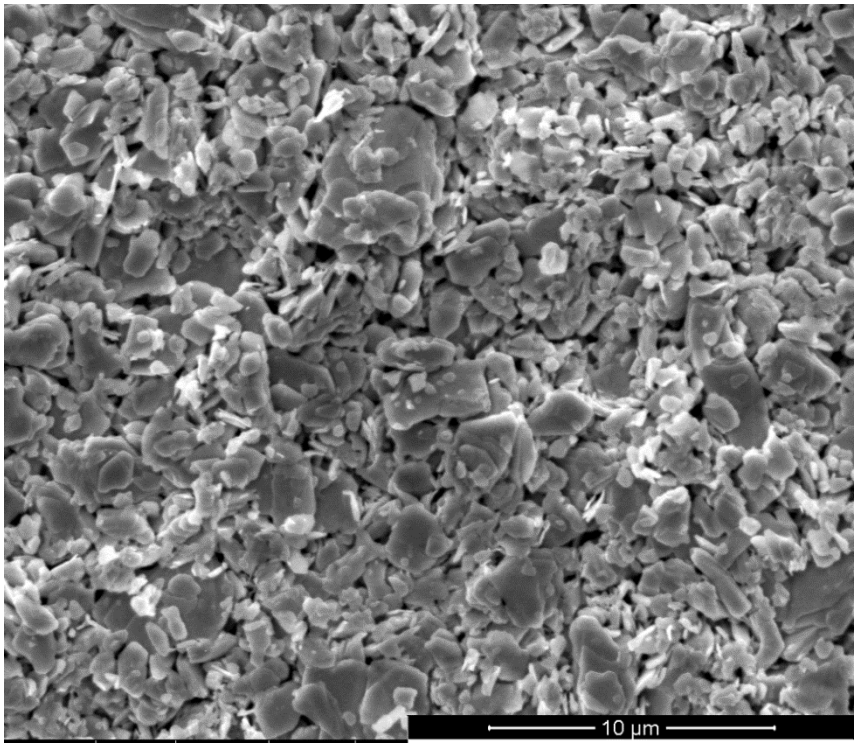

Figure 16: Micrograph of ETP pressed at 20 KSI showing clear texture of Bi-2212 and interspersed silver nano-powder.

The test pellet held the pressed shape, all though it still had the same fragility that has plagued all Bi-2212 development. The texture of the pellet was then viewed under a SEM and it was obvious that the texture was maintained as the micrographs looked nearly identical to the one performed in the textured powder study, except for the presence of silver particles. Figure 16 shows a micrograph of an ETP pellet before heat treatment. Due to this nearly identical match, X-ray diffraction was not used to re-measure the texture parameter.

A small pellet with four silver tabs was fabricated by a colleague Dr. Nathaniel Pogue to be used in a test to it if it is capable of carrying a supercurrent after heat treatment. The pellet was heat treated with a simple heat treatment to a maximum temperature of 875 C for 24 hours using typical Bi-2212 ramp rates, but without an annealing step or in properly controlled environment during heating. The sample was then cooled in a liquid helium bath (4.2 K) and a resistivity test was performed. Figure

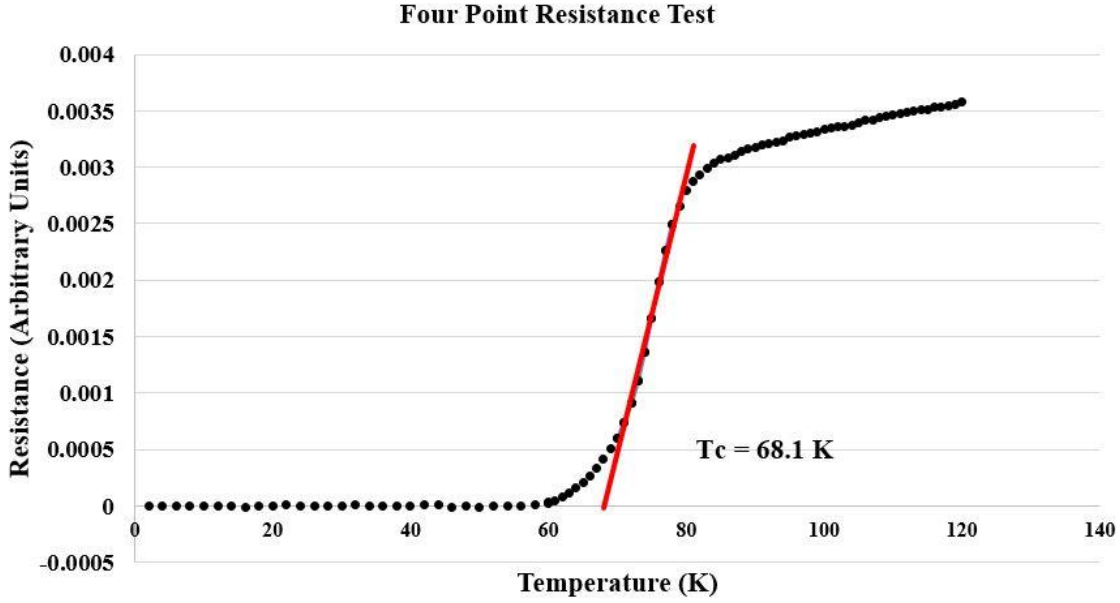

Figure 17: Four point resistance test showing critical temperature at 68.1 K

17 shows the results of the test confirming that the resistivity of the pellet did drop to nearly zero. It however is obvious from the test that process development was necessary as the transition temperature is at 68.1 K when it should be at ~85 K.

With the ability to carry supercurrent verified a series of heat treatments was necessary to check the feasibility of melting the local regions where Bi-2212 and silver are in contact without melting the bulk of the BSCCO. To do this pieces of coined pellets containing 5% silver and pure Bi-2212 were heated side by side on silver foils to test the melt temperature of each. Melting was verified simply by viewing when the sharp edges of the pellets soften, and growth halo of the crystalized Bi-2212 is viewed along the base of the pellet. Table 3 shows the results of the melt temperature comparison study and Figure 18 shows samples of the enhanced pellets alongside pure

Table 3: Results of the melt temperature study comparing the behavior of ETP and pure samples after being textured.

Melt Temperature Study			
Max Temperature (C)	Powder Type: Pure/ETP	Halo	Edges Melted
879.1	Pure ETP	No Yes, but only slight	No No
879.2	Pure ETP	No Yes	No Yes
879.9	Pure ETP	No Yes	No Yes
880.1	Pure ETP	Yes Yes	Yes Yes
880.3	Pure ETP	Yes Yes	Yes Yes
880.8	Pure ETP	Yes Yes	Yes Yes

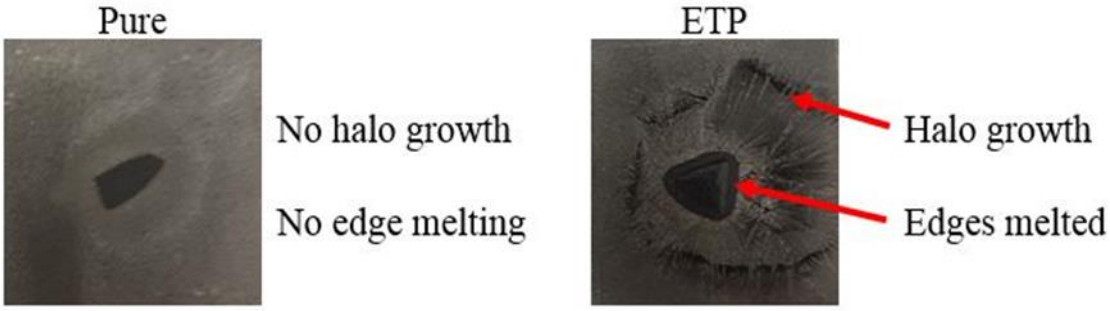

Figure 18: Comparison of pure and ETP textured pellet samples heat treated to a maximum of 879.9 C. Notice the pure sample has no indications of melting while the ETP sample show both edge melting and crystal halo growth along the silver foil.

counterparts. The enhanced pellets were found to begin melting a full 1.0 C below the pure samples. This shows that it is feasible to locally melt the silver-BSCCO boundary without melting the bulk.

Now that the melt temperature of the enhanced powder was found, verification was needed that adding silver nano-powder would facilitate grain growth and

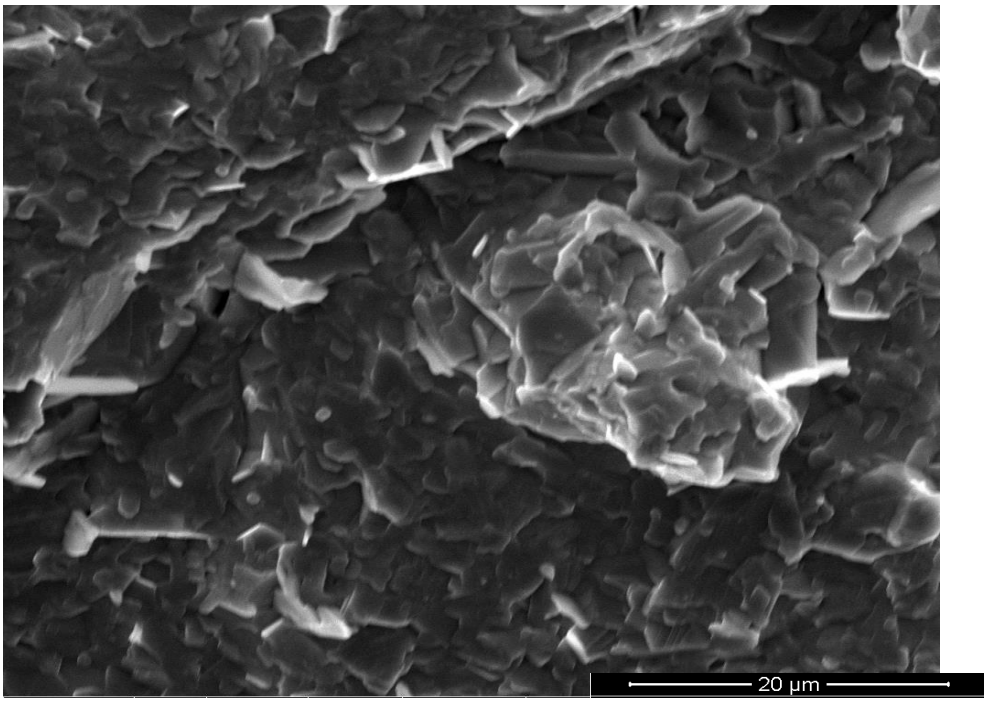

Figure 19: Micrograph of ETP pellet heat treated to a maximum temperature of 878 C. Significant grain growth and interconnectivity are evident.

interconnectivity. Pellets were heated to 879 C and below using conventional ramp rates and view under an SEM. Figure 19 shows a micrograph images displaying significant grain growth and interconnectivity that was not present without the silver nano-powder enhancement. These initial tests showed that not only was this method was a possible route to a non-melt heat treatment for pre-textured Bi-2212, but that a reasonable maximum heat treatment temperature region (877 C – 879 C) existed that would produce the desired effects.

3. ETP BAR AND WIRE PROCEDURE*

The procedure for creating the ETP bars and producing multifilament wires from them has a multitude of steps and pitfalls that require careful attention. This section will provide an abridged breakdown of this procedure, including powder handling, ETP bar fabrication, ETP bar and silver matrix preparation, and wire drawing. While this section does include all highlights and necessary information to understand the process, it is not meant as step by step instructions to recreate the procedure. The entire step by step process of creating ETP bars developed for this work can be found in Appendix A.

The Bi-2212 powder must be handled in a manner that minimizes its exposure to air and moisture, as it will absorb both carbon dioxide and water from its environment. The carbon dioxide will poison the superconducting properties if it is held in the material during heat treatment [82], even more catastrophic is if carbon dioxide, or moisture volatilizes during the heating and causes void spaces or a burst in the wire [81]. Several precautions were taken during the course of this work to limit the exposure to the Bi-2212 to the environment. The phase pure Bi-2212 powder is calcined to remove moisture and carbon dioxide at 800 C. After calcination all powder is immediately placed inside of a nitrogen glove box. All measuring and handling of the powder is done inside the glovebox from this point on, or in containers that are sealed when inside the glove box. The correct amounts enhanced powder is measured and removed from the glovebox as it is needed.

*Part of the data reported in this section is reprinted from J N Kellams *et al* Presented at the 2015 CEC-ICMC, Tucson AZ, USA [102]

*Part of the data reported in this section has been submitted for publication and reprinted from J N Kellams *et al* Presented at 2018 ICEC-ICMC, Oxford, England

Two different sizes of silver nano powder (20 nm and 100 nm) at two different concentrations (3% and 5% by weight) were homogenously mixed with phase pure fine (~ 1 μm) Nexans Bi-2212 powder. Table 4 shows the different concentrations and sizes that were used. The purpose of using different sizes was to ensure that the powder would be homogenously mixed, but since even the larger of the silver powders is still significantly smaller than the Bi-2212 powder it proved to have no effect on the ability to be mixed. Originally the different concentrations were going to be used to test if it would have any effect of the overall current carrying capacity of the final wires, but complications and process development caused this to be pushed to a potential future work. The mixing was done using a Resodyn mixer operating at an acceleration of ~ 20 g's. The silver powders for all concentrations and sizes mixed well without any problems. Refer to section 2 for figures of the homogenously mixed Bi-2212 and silver nano-powders. The sealed containers are then stored in the glovebox until they are needed to press a bar.

Table 4: Silver nano-powder size and mixture concentrations for enhanced Bi-2212 powders.

Mixture	Ag weight %	Ag particle size
Large 3%	3%	80-100 nm
Large 5%	5%	80-100 nm
Small 3%	3%	20 nm
Small 5%	5%	20 nm

Each bar takes approximately one full day to fabricate, including the time necessary to clean the die parts in between each bar being pressed. This long production

time coupled with the tendency of the original process to yield cracked or completely broken bars upon opening the die resulted in a need for significant process development. The die was designed so that opening it would not disturb or shock the coined bars after pressing, but did not anticipate other factors. The original design did not completely accommodate the abrasive nature of the Bi-2212 powder or the effect of the large volume reduction during compression. It also did not anticipate some of the more intricate details involved in applying uniaxial compression to a ceramic powder. Several modification to both the process and the die were necessary to increase survivability of the bars and thereby reduce the overall production time.

The enhanced textured powder bar pressing process involves pouring 9.3 grams of enhanced Bi-2212 powder into the female die form. To facilitate even distribution of powder in the 4 mm a special powder slide was made. Figure 20 shows the female die half assembled and the slide being used to fill it fully assembled. The female die is then

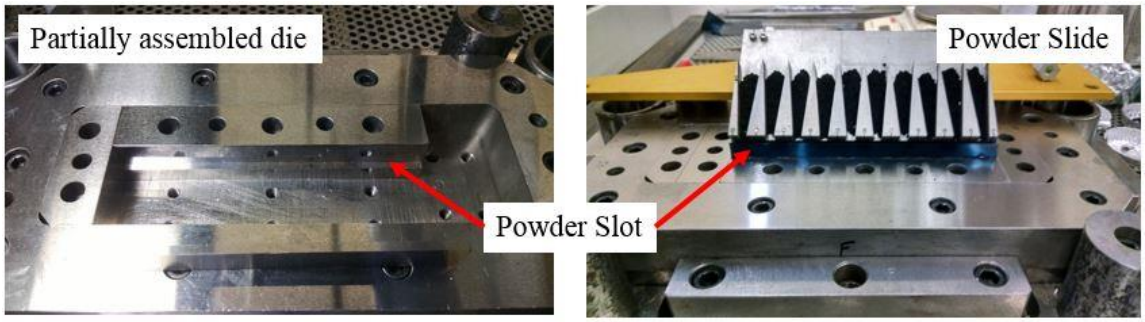

Figure 20: (Left) Image showing the partially assembled die to illustrate the position of the powder slot. (Right) The powder slide loaded with enhanced Bi-2212 fine powder before evening filling the powder slot.

positioned and aligned under the hammer assembly inside a large hydraulic press, shown in Figure 21. A plastic tent is then placed around the die and purged with dry argon until the die is removed from the hydraulic press for extraction of the bar. The enhanced

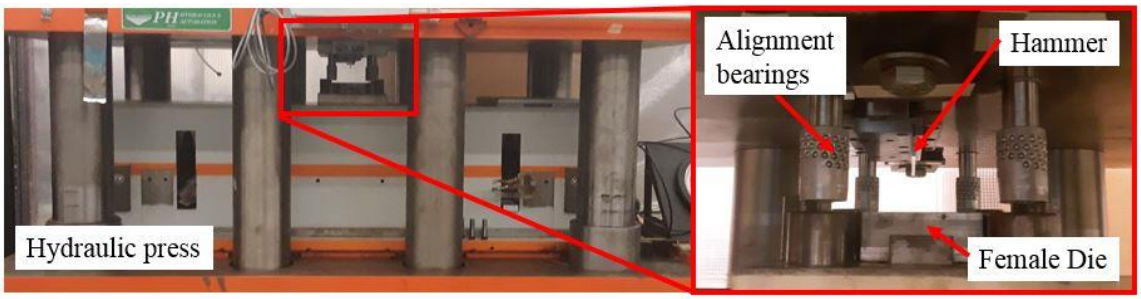

Figure 21: (Left) Both female die and hammer positioned in the hydraulic press. (Right) The fully aligned die before pressing.

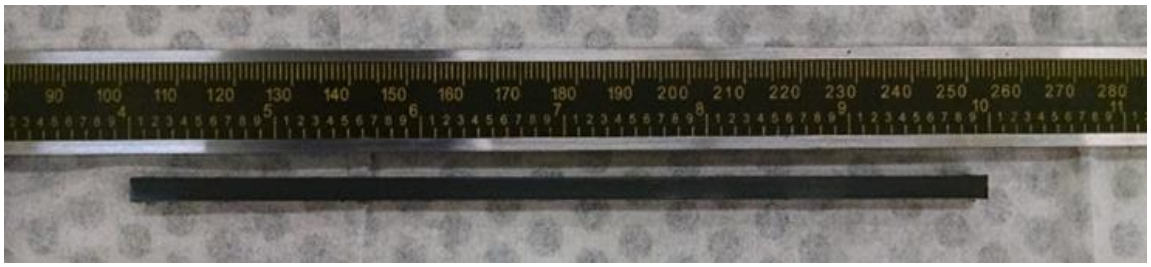

Figure 22: ETP bar after removal from the die.

powder is uniaxially compressed at 20 KSI to create a (4 x 4 x 150) mm bar of compressed enhanced Bi-2212 textured powder, shown in Figure 22. It was noticed that when performing the pressing, the pressure would build up and drop when the male die lowered. This strongly indicated the die was sticking during operation, but upon further inspection it was not the male die sticking to the female die. The Bi-2212 was galling the polished surface of the die in a way that was causing the die to stick as it lowered. Figure 23 shows galling of a female die piece located at the end of the bar. It was concluded that as the male die was compressing the powder on the top and texturing it first, this combined with the increased pressure caused the micaceous flakes of Bi-2212 to dig into the sides of the female die and then eventually break free as it was pressed further. This left Bi-2212 powder embedded in the hardened steel surface. The damage to the die was noticeable, but not restrictive to the process unless it continued. To alleviate this issue to the width of the die blades were ground down by 0.005 inches to

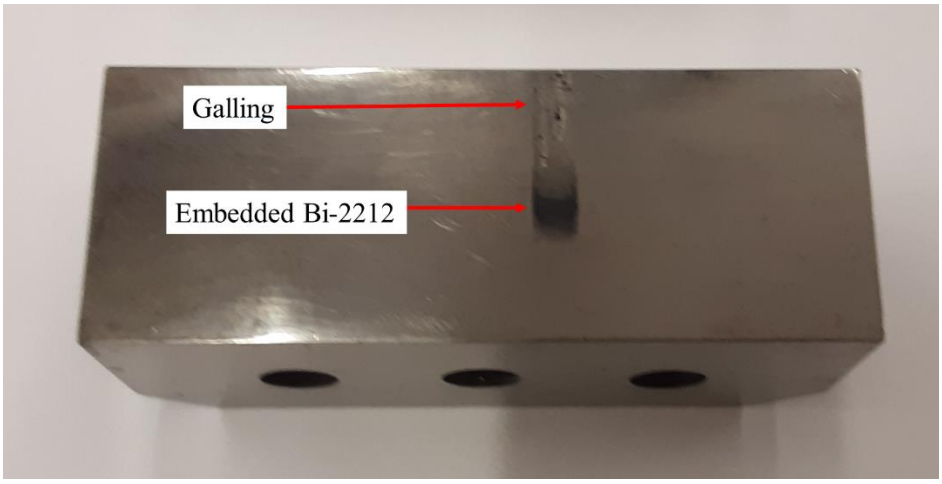

Figure 23: End piece of the female die showing galling and embedded Bi-2212.

accommodate a 0.002 inch thick steel foil on either side of the powder in the die, to act as a protective layer between the abrasive powder and the female die. This addition protected the die but caused another issued. As the die was lowered, instead of simply digging into the protective shims and breaking free as it did without the protective shims, the Bi-2212 powder would grab onto the steel shims and dragged them down as the powder compressed. This causes the steel shims to buckle and become imbedded within the pressed bars. Figure 24 shows a steel shim embedded within an ETP bar. This

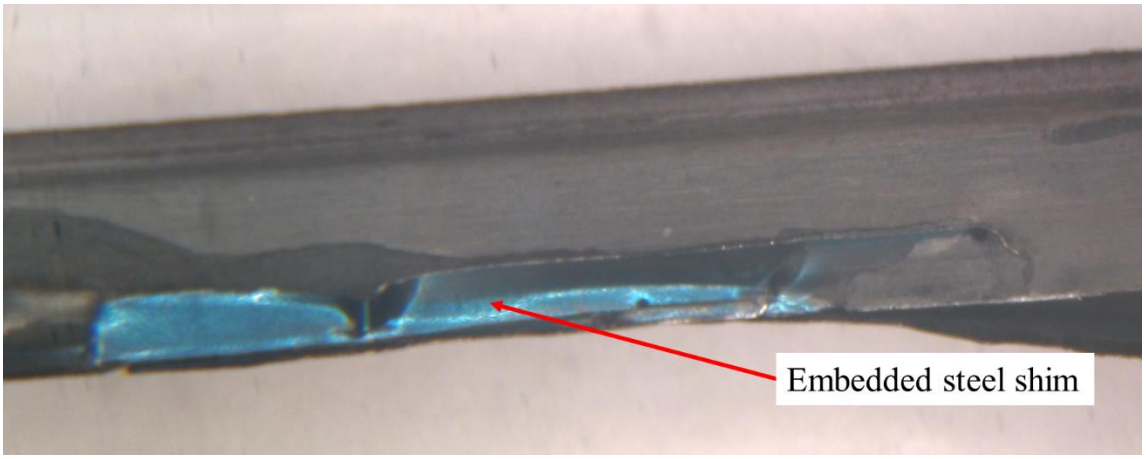

Figure 24: Close up of an ETP bar with an embedded blued steel shim.

obviously is not acceptable for the core of a superconducting wire, so the anvil located at the bottom of the female die was also ground to allow the shim room to be dragged down with the BSSCO powder without buckling or imbedding into the Bi-2212 bar. Figure 25 shows a diagram of the shims and how they function to protect the die while not sacrificing the ETP bars. This significantly increased the survivability of the ETP bars to above 90%, where every broken bar could be attributed to a slip of the hand

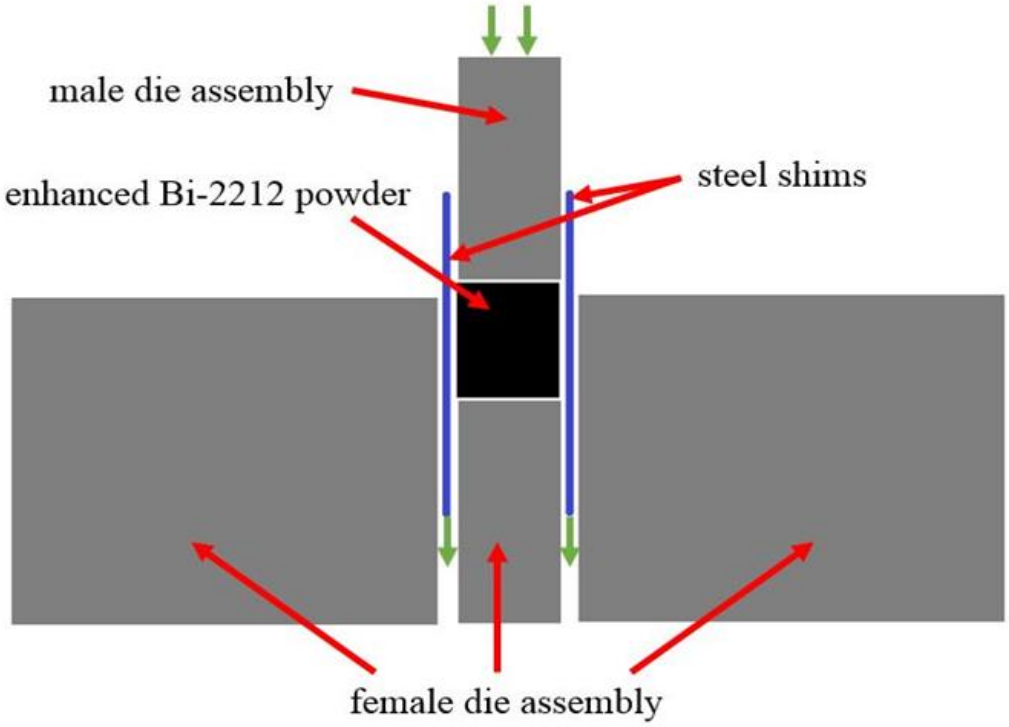

Figure 25: Illustration of the placement of the steel shims in the die assembly.

during extraction or die pieces sticking together during disassembly due to spillage of the Bi-2212 powder during filling.

Once the bars could be reliably fabricated without breaking, a common attribute of the full length bars revealed itself. The bars each had a curvature of ~2500 mm, this may seem slight but the silver sheath tube drawn to house the ETP bars was made only

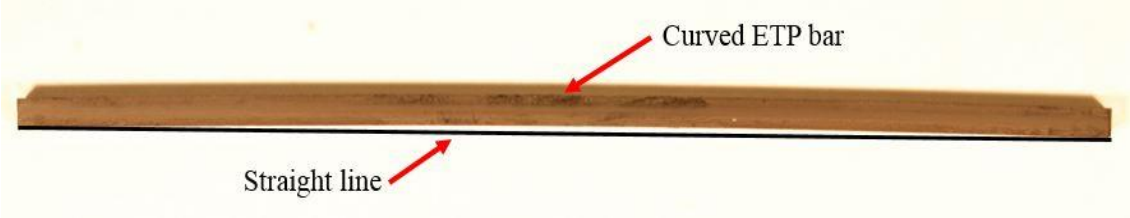

Figure 26: Curved ETP bar with a superimposed straight line to illustrate the curvature.

slightly oversized to reduce to the chances of damage to the bars during wire drawing. Figure 26 shows a photograph of a curved bar with a straight line superimposed to illustrate the curvature. The sheath tube was too tight to fit the curved ETP bars without breaking them, and even if it would fit, leaving it curved would not work with developing this process as a basis to create long lengths of wire. The curved bars could cause breaks and potential gaps during wire drawing process if not remedied. The pressing procedure would have to be altered again to produce a straight Bi-2212 bar without forfeiting the previously mentioned changes.

The curvatures form due to a density differential and the resulting internal stress differential that can form when uniaxially compressing ceramics [103]. The proper solution to this problem is to compress the ceramic powder (BSCCO) using a dual action die. This was not feasible for the scope of this project, as it would require a completely new floating die design. Instead a stop-gap solution was used. By cutting new hammer and anvil pieces of the die with a counter curve to offset the curve found in the bar, the process yielded a straighter bar. The steps of measuring and cutting new hammer and anvil die pieces continued for 3 more iterations, until the bar was straight. The final die

pieces had a counter curvature of 4500 mm to offset the initial ~ 2500 mm measured curvature of the bar.

The final step of the ETP bar process involved shaving the four long edges from the bars to allow the bars to fit into the silver sheath. The drawing processes for creating the square centered silver tube involves drawing the tube with a floating square mandrel. The mandrel had slightly rounded corners that obviously resulted in rounded corners on

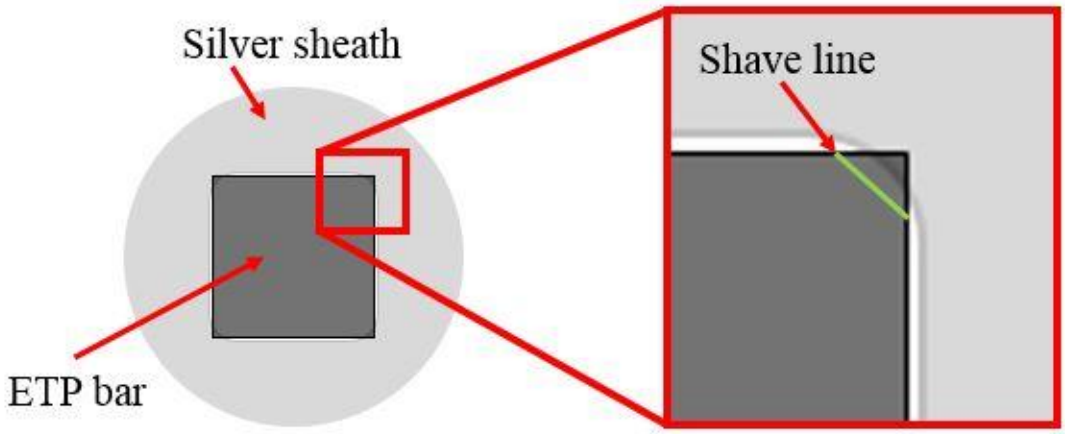

Figure 27: Illustration showing the corners of the ETP bars that needed shaved off to fit into the silver sheath tube.

the square section of the inside of the tube. These rounded corners would not allow the ETP bars to slide easily into the sheath and needed rounding. Figure 27 shows a cross-sectional diagram of an ETP bar superimposed on the silver sheath tube. This process proved to be exceedingly difficult and had a very low survival rate of the bars. The bars were placed into a precision V-groove and scraped with a razor blade, to add to the difficulty of doing this without shocking or vibrating the bar this process needed to be done inside of a glovebox to limit the exposure to air and moisture. The V-groove was made in two pieces that were locked together transversely by standard key stock. One piece of the fixture held the ETP bar so that the edge could be shaved. The groove was

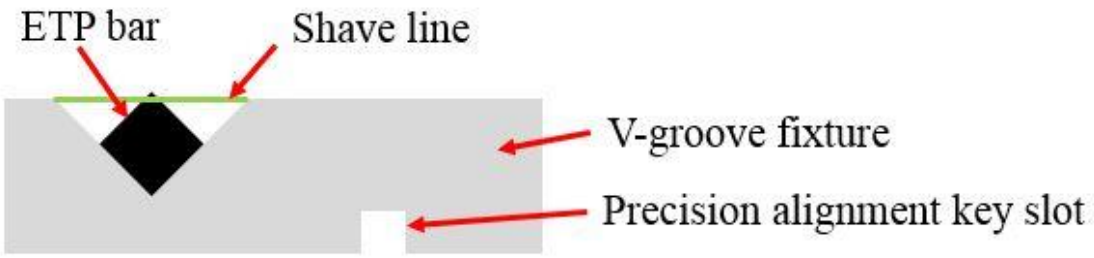

Figure 28: Diagram of V-groove fixture for shaving ETP bar edges to fit into silver sheath tube.

precision cut so that the edge of the bar would be shaved until it was flush with the top of the fixture. The bar was then rotated and the next edge was shaved unto all four were completed. This step of handling was the most likely place for a break to occur. Figure 28 shows a diagram of the first piece of the fixture. The second piece of the fixture held the silver sheath tube so that the center line of the tube was lined up with the center line

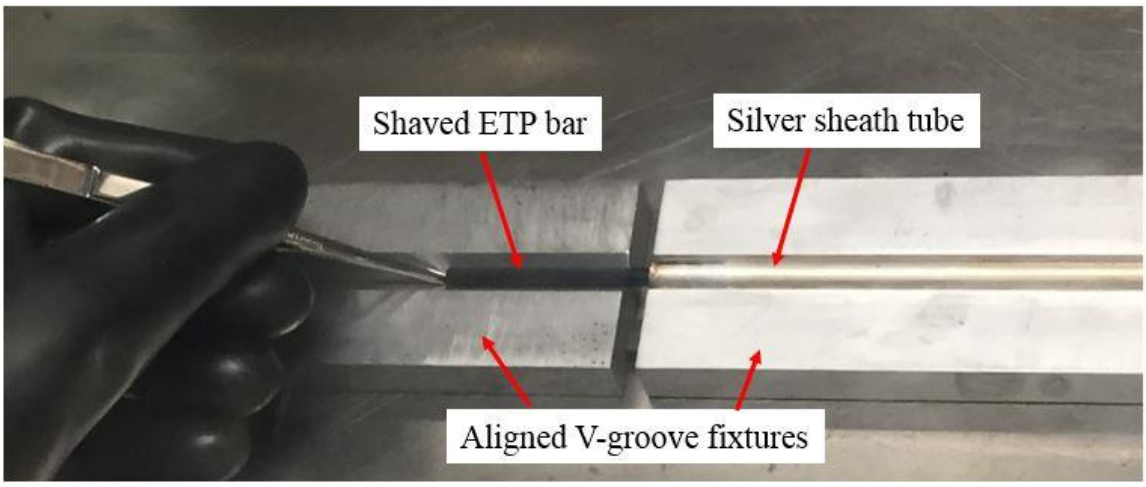

Figure 29: Shaved ETP bar being inserted into silver sheath tube using aligned V-groove fixtures.

of the bar. Once all four edges of a bar were shaved it was simply pushed into the silver sheath tube. Figure 29 shows a photograph of a bar being pushed into the sheath tube using the V-groove fixture while inside a glove box. The survivability of the bars through the shaving process was much lower than would be allowable for any reasonable

production. Luckily, the solution to this problem is simple if you know about the problem before the silver sheath tube is made. Simply, draw the silver tube with either a different or slightly larger mandrel so the ETP bars can easily fit into the sheath.

To prepare the silver sheath tube before the ETP bars are inserted it was etched in a nitric acid solution to remove surface tarnish and then stored in alcohol during transport back to the glovebox. The alcohol was allowed to evaporate off of the sheath in a nitrogen environment before being placed into the glovebox. Inside the glovebox, using the method described above the bars are were placed end to end in the silver sheath. One of each concentration and size mixture of silver nano-particles was used. The ends of the sheath were hot glued to seal the silver tube as well as keep the bars from moving longitudinally. The silver sheath was marked at the locations of the butt joints between the individual bars inside the sheath. The billet was then drawn down so that the silver sheath was barely touching the Bi-2212 bars locking them into place. At this stage the billet is drawn down into a wire using ~10-15 % reductions at each step.

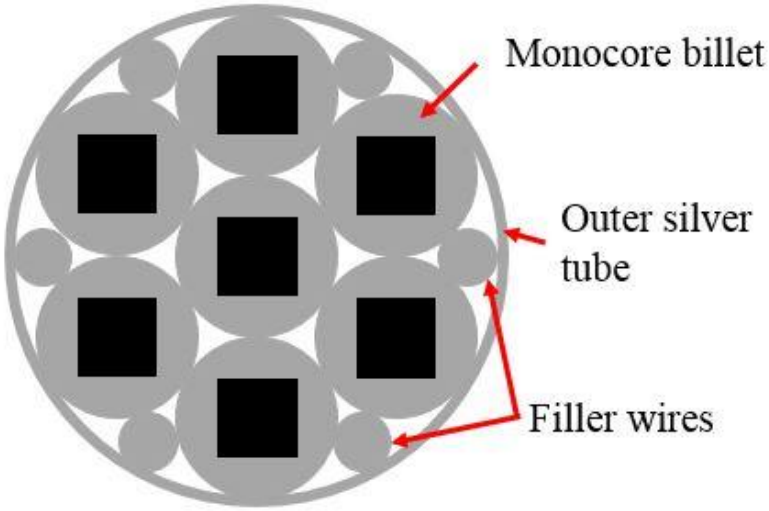

Figure 30: Stacking pattern of monocore billets and filler wires for a 6-on-1 multifilament wire.

When the monofilament wire was drawn to a sufficient length it was cut at the marked points to separate the different sizes and concentrations of silver in the enhanced textured powder cores. Because the process of drawing the monocore wire went so smoothly it was decided to go ahead and attempt to restack and draw again to create a 6-on-1 configuration of wire. The monocore of each type were cut into seven 12 inch segments, straightened, and the ends were sealed. These segments along with filler wires were etched in nitric acid and stacked into the pattern shown in Figure 30. The filler wires close the gaps between the monocore billets to maintain the shape of the superconducting core cross section during the drawing process. That entire package is inserted into a thin walled silver tube and draw down until the desired size is reached. Figure 31 shows the cross section of the 6-on-1 wire after drawing, notice the cross section of each individual filaments is still approximately square. This was not the case for the previously developed extrusion/drawing process where even the monocore was

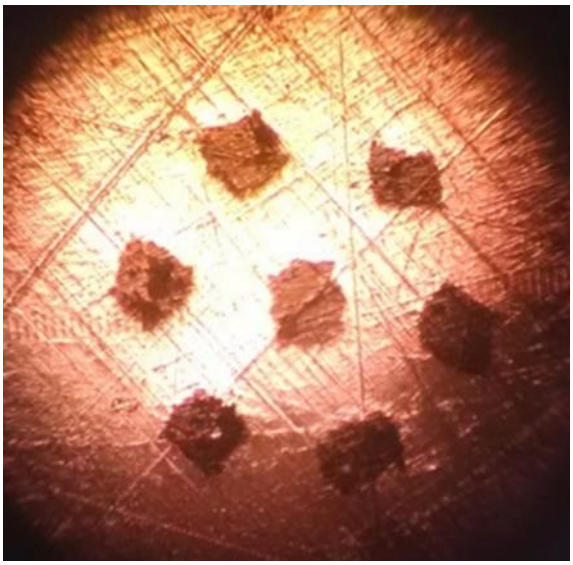

Figure 31: Cross-section of 6-on-1 multifilament wires, showing filaments with only slight deformation.

drastically deformed after the wire was drawn. The draw bench that was used for this project was limited to ~50 feet, so large section were cut off at various sizes and the rest was drawn down further. This procedure was repeated until the final wire was drawn down to have a wire diameter of 0.8 mm. This resulted in having ~10 ft sections of decreasing wire diameters. Some of the 6-on-1 wire was restacked and drawn again to create a 7 x 19 format. Figure 32 shows a diagram of the 7 x 19 layout as well as a cross section of the wire.

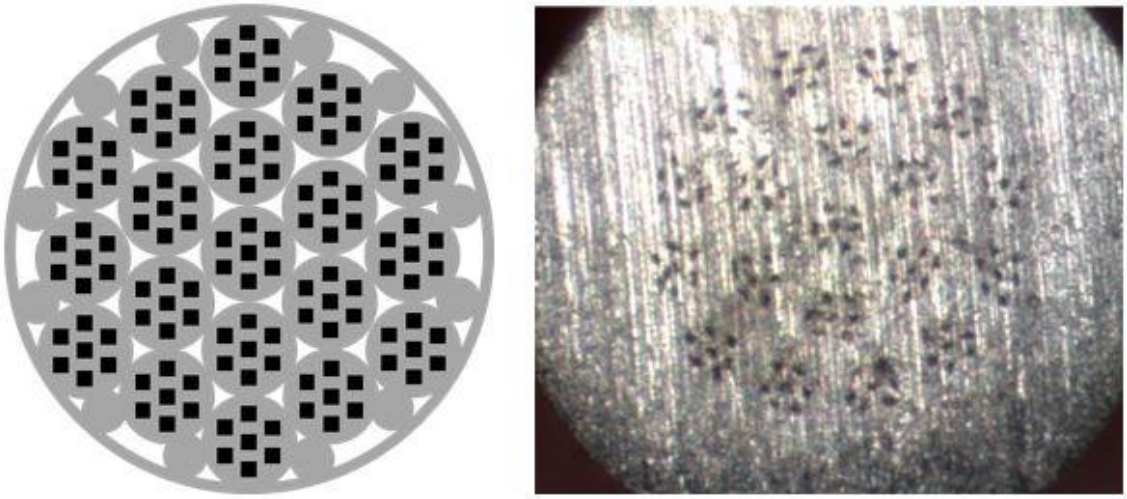

Figure 32: (Left) Diagram of stacking pattern to draw 7 x 19 wire. Cross-section of 7 x 19 multifilament wire.

The entire drawing process completed without a single break in the wire. This is believed to be due to the pre-texturing of the micaceous powder. Even in the compressed state the flakes can easily glide across one another longitudinally during the drawing process, allowing the bar to spread as the silver sheath is stretched. This attribute also kept the ends of distinct bars from separating during the drawing process, and instead allowed the ends to smear together creating a near seamless joint between the bars. This smearing can be considered as an analogy to laminar flow, where the Bi-

2212 near the surface of the silver matrix is dragged with the silver, and each layer of the Bi-2212 moves less as the center of the filament is approached. Further investigation will be necessary to verify this hypothesis, but for this work it is sufficient that multifilament sub-millimeter wire was able to be drawn without incident.

4. HEAT TREATMENT STUDY AND TEST SETUP*

A crucial component to this work is the development of the non-melt heat treatment. Initially, a heat treatment schedule was taken from the literature and used as a basis for temperatures and times on factors that would be similar between the widely accepted partial melt process and this works non-melt process [92]. The similarity between the two methods are the ramp rates up to, and down from, the maximum temperature that allows for optimum crystal growth. The changes to the heat treatment schedule for this work required that the maximum temperature be lowered below the partial melting point of Bi-2212, the time at maximum temperature be altered to allow all Bi-2212/Ag interfaces to melt without melting the bulk of the superconductor, and finally the anneal temperature was altered to adjust for results from studies on anneal temperatures effects on critical current [104]. The studies that were performed to systematically alter the parameters were performed in two main phases. The first phase was heat treatment of short sample multifilament wires, and the second phase was the heat treatment of individual ETP bars. The supercurrent carrying test results will be discussed in section 6. This study was devised in a way that allowed the critical current test to be performed in liquid nitrogen rather that in liquid helium. However, due to the residual resistances in Bi-2212 that can be high at liquid nitrogen temperatures this test is really only applicable for comparing the samples within the study and not for comparing this method of preparation to other methods. Comparison with other methods of preparation will require optimization of the heat treatment in liquid helium.

*Part of the data reported in this section has been submitted for publication and reprinted from J N Kellams *et al* Presented at 2018 ICEC-ICMC, Oxford, England

The initial heat treatments were performed in a small table top furnace. This obviously would be unsuitable to heat treating any length of superconducting wire. A larger quartz tube furnace would be used to heat treat the ETP wires and bars for this work. However the larger furnace needed to be upgraded with an Omega CN7800 controller, since the original controller was only accurate to +\- 2.0 C. Both furnaces are shown in Figure 33. The upgrade allowed the controller to be trained with the treatment

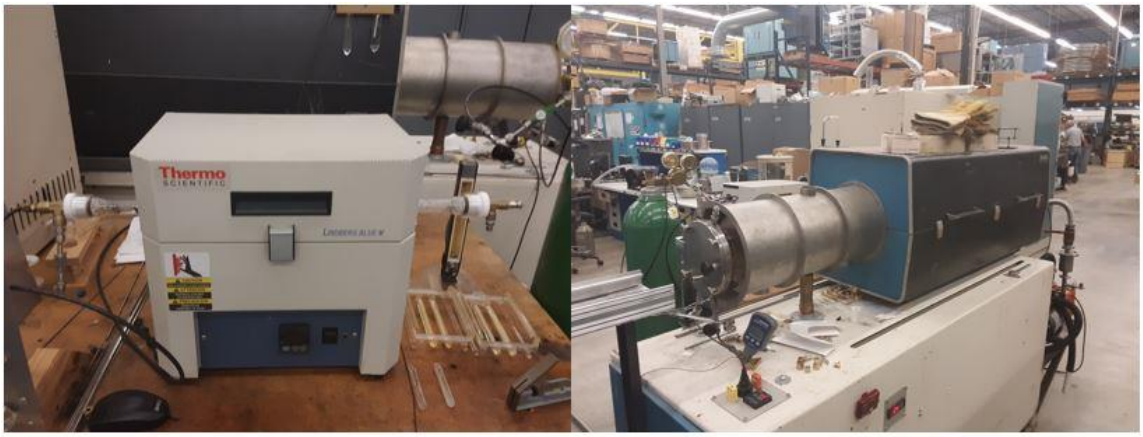

Figure 33: (Left) small furnace used for initial tests. (Right) Furnace used to develop non-melt heat treatment of ETP bars and wires.

profile so that the temperature accuracy was +\- 0.1 C in the center of the heating region. In addition to this special baffles made of oven brick and silver reflector needed to be made to flatten the temperature profile of the furnace to allow a uniform region to place the samples in. Traditional steel baffles cannot be used due to the high temperatures and an oxygen environment. Figure 34 shows a five inch region of +\- 0.2 C uniformity with the baffles in place. Due to this limitation all samples were made to be less than 4 inches long and were centered in the uniform region during heat treatment.

Heat treating the multifilament ETP wires unveiled several addition complications that were not present during the initial heat treating of the ETP pellets.

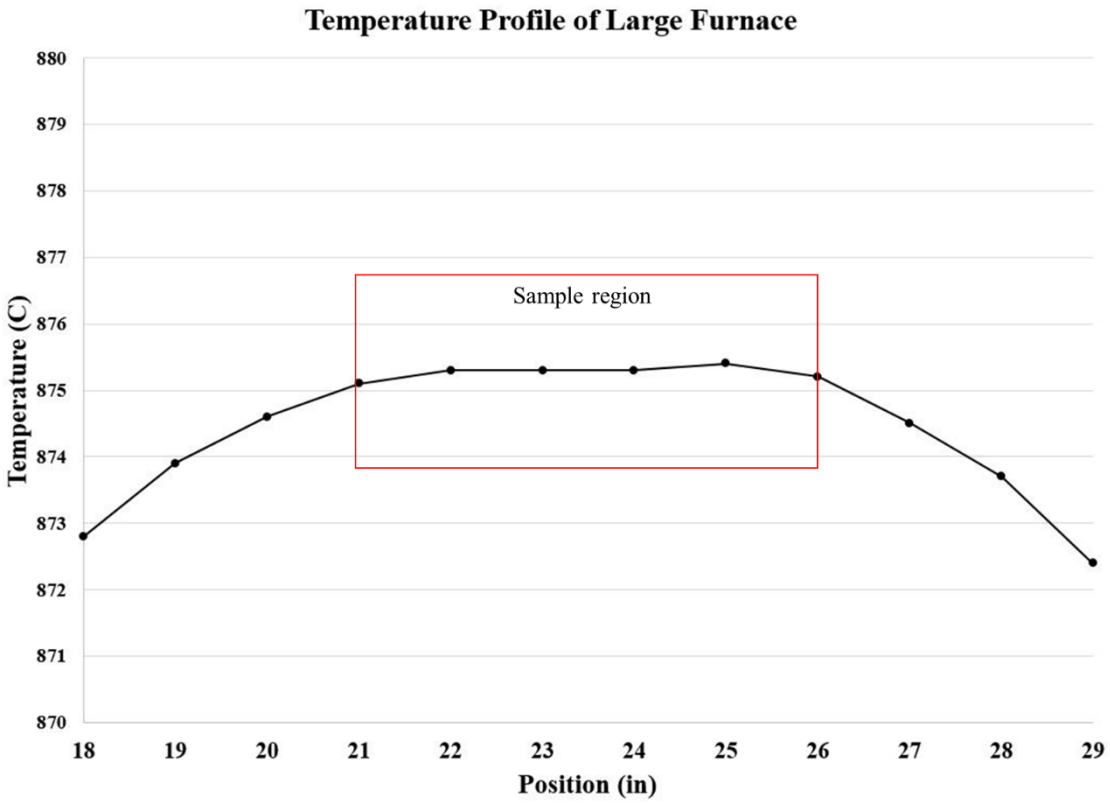

Figure 34: Temperature profile of the large furnace including the sample region.

Firstly, completely sealing the ends of the short sample wires proved exceedingly difficult. Figure 35 shows a typical leaked end. The first attempt to seal the ends involved hammering the ends closed after clipping the wire ends. The idea was that the filaments would collapse when hammered closed, but the liquid Bi-2212 proved to be to chemically aggressive enough that any miniscule path through the hammered end prevented sealing. The second attempt involved dipping the clipped ends in molten silver to provide an actual cap to the end, but this method only worked a portion of the time as a small amount of Bi-2212 powder would melt when the end was dipped leaving behind a filamentary path through the cap when it solidified. Finally, a combination of the two methods was used. The approach was to hammer the end closed, dip that into

the molten silver, hammer any filamentary path that appeared, and then dip again so that a liquid tight cap would be formed. Figure 35 shows a dipped endcap clearly showing a visible Bi-2212 liquid film that solidified. In addition to capping the ends, the wire was

Figure 35: (Left) Typical leaked end of hammered end. (Right) Hammered and dip coated end showing very slight Bi-2212 film after heat treatment.

later coiled in a manner that would impede leaking while simultaneously significantly lengthening the sample reducing the likelihood that and leaking from the end would affect the central portion of the wire sample. It was found that the end leaking and any residual Bi-2212 would cause the sample to bond to the ceramic surface of the boat where the Bi-2212 touched it. Initially, it was attempted to place silver foil between the boat and the sample but this was ineffective at preventing the fusing of the surfaces. Finally, sacrificial ceramic pieces were placed under the wire sample and left fused to the sample throughout the entire cooling and testing procedures. It is not anticipated that this will be a future problem as long length wires can be configured to leave long stingers of wire outside of the hot region of the furnace thereby maintaining a seal on the end with cool, solid Bi-2212 as is typically done with Bi-2212 wires [105].

Bi-2212 at liquid nitrogen (LN) temperatures tends to have relatively high residual resistances, this combined with LN being very close to the transition

temperature of Bi-2212 made it difficult to perform this test on multifilament wires. Initial tests of the multifilament wires showed no superconductivity. Each of these initial tests simply showed the resistive V-I line that was approximately equivalent to the resistive line that the silver matrix alone would produce. No difference could be seen between the different heat treatments of the ETP multifilament wires. It was unknown if the filaments were even in a superconducting state or if the residual resistances were simply higher than the resistance of the silver matrix. To remove the complication of the silver matrix and allow results to be measurable, special ETP bars were pressed with isolated silver tabs imbedded into the bar, shown in Figure 36. These tabs allowed for current leads and voltage taps to be easily soldered to the ETP bars for testing. The heat treatment study performed on the ETP bars served several purposes. It allowed a systematic study of the effect of maximum temperature on the capability of similarly prepared samples to carrying supercurrent, and allowed to verify a non-melt heat treatment would even allow for a significant supercurrent transport.

Figure 36: ETP bar with embedded silver tabs as solder points.

Each silver tabbed ETP bar and wire was heat treated according the schedule shown in Figure 37 with maximum temperature being the variable between heat treatments. The choice of maximum temperatures were chosen based off of the study done in section 2 in which samples of both pure Bi-2212 TP, and ETP pellets were

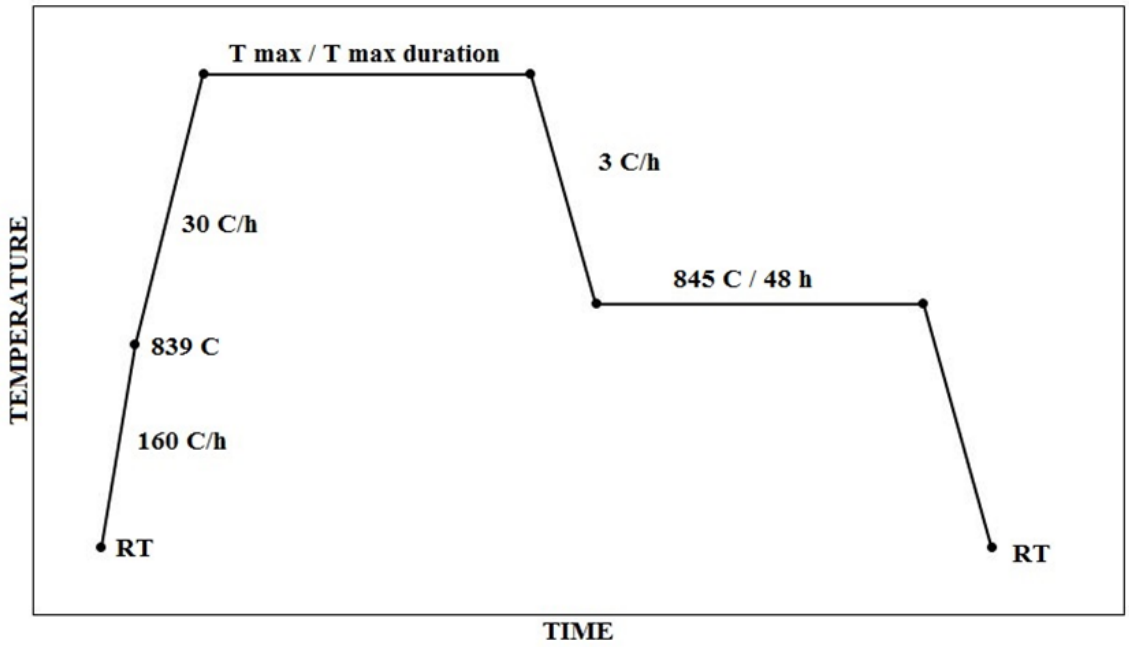

Figure 37: Heat treatment profile used for both ETP bars and ETP multifilament wires.

simultaneously heat treated to find the temperature that each begin to show signs of melting. The range to be tested then had a maximum temperature at which the pure ETP pellet began to show signs of bulk melting and was stepped down by 0.5 C increments until well below were any superconductivity would be expected. The ETP bars were heat treated in silver boat on a bed of enhanced textured powder. This is done because the presence of extra silver from the boat can alter the outcome of the heat treatment. Figure 38 shows the difference between the free top and bottom that was sitting on silver of a single pellet. All ETP bars and wires were heat treated in 1 atm of oxygen until the beginning of the annealing plateau when the furnace was purged with air and allowed to conclude the heat treatment schedule open to the air. This is done to remove any excess oxygen that is over doping the samples.

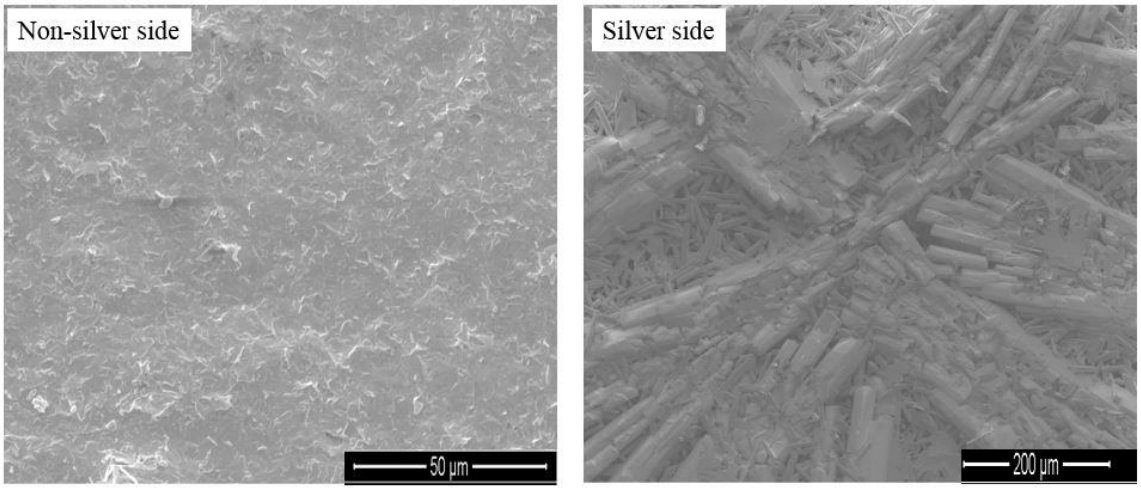

Figure 38: Micrographs comparing non-silver side and silver side of an ETP pellet heat treated to a maximum temperature of 879.5 C. Notice the large irregular crystal growth of the silver side compared to the interconnected grains of the non-silver side.

A simple top hat was designed and built for use in a 5 L liquid nitrogen Dewar, in a way that could be used for current testing both the ETP bars and short sample wires in a LN bath. Figure 39 shows the top hat and Dewar, including the sample holder. A 1 kA HP power supply was used to drive current during testing and two HP multimeters read voltage. Two voltmeters were used for the dual purpose of verifying measurements and measuring different regions of the wire independently. The ETP bars and wire were attached to the current leads via a broad silver foil to the outer silver tabs, and one pair of voltage taps attached to the inner silver tabs. Once all leads and voltage taps are securely soldered the top hat is lowered into the Dewar and pre-cooled in nitrogen vapor. The pre-cooling served to prevent thermal shock of the fragile superconductor when being bathed in LN. Once the sample was cooled to 77 K the current through the sample was slowly increased. The test was terminated when a very clear transition or resistive line was observed and the data was recorded for later analysis.

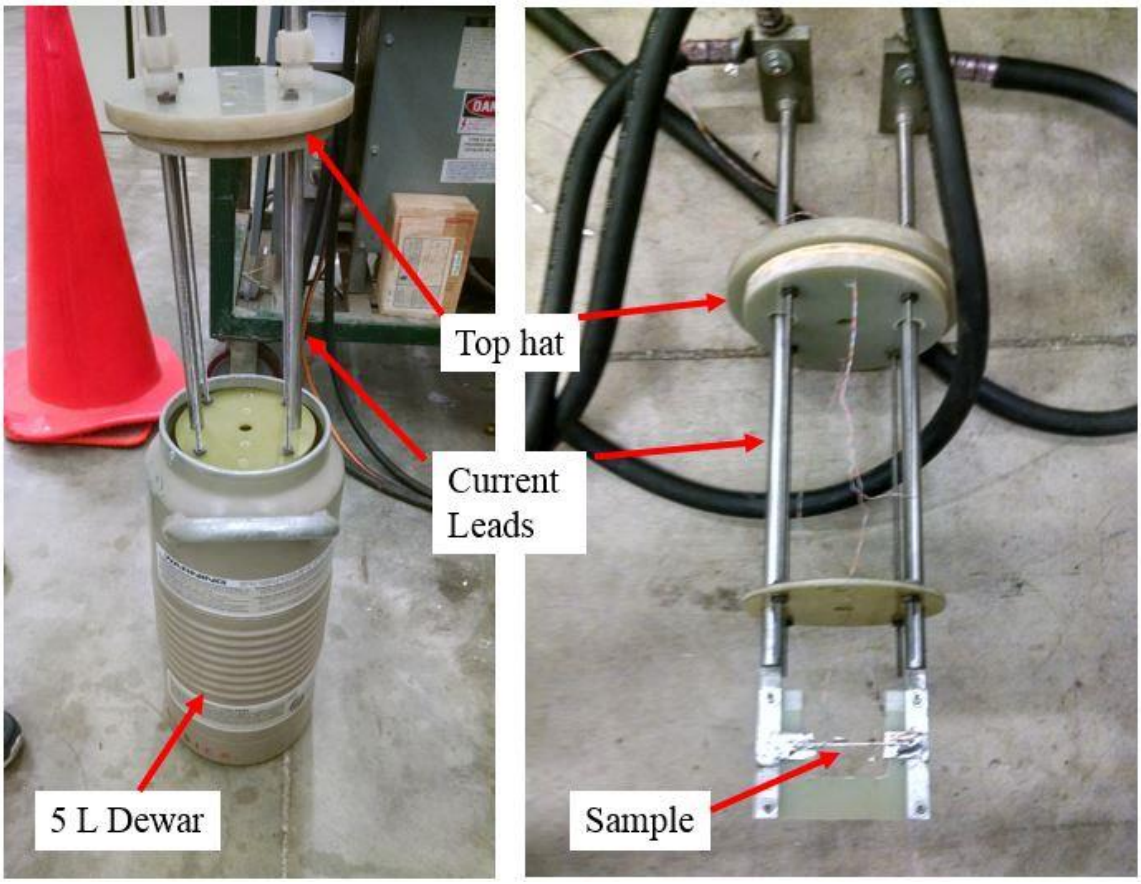

Figure 39: (Left) Top hat partially inserted in 5 L liquid nitrogen Dewar. (Right) Top hat showing sample attached to current leads before testing.

The purpose of the current tests on the ETP bars were twofold, the first being to verify that the non-melt heat treating method was producing a superconducting material at liquid nitrogen temperatures. Since the transition temperature of Bi-2212 is 85 K any significant deviation of oxygenation during heat treatment could yield a material that has a critical temperature below 77 K. Secondly, upon verification of superconductivity the tests would confirm that a maximum temperature band of non-melt temperature heat treatment could produce a material with the capability to carry supercurrent.

5. ETP TRANSITION TEMPERATURE*

The initial verification of supercurrent transport was done on a four tab pellet tested in liquid helium. It displayed a transition temperature that was significantly lower (68.1 K) than the expected 85 K for Bi-2212. The lowering of transition temperature in Bi-2212 primarily is caused by the doping of oxygen in the crystal, with any under or over doping resulting in a significant lowering of critical temperature [106]. Since initial current tests of multifilament ETP wire showed no superconductivity in liquid nitrogen, an ETP bar was setup for testing as described in section 4, but instead of increasing the current over time a thermocouple was placed on the bar and the sample was allowed to slowly warm over the course of several hours. Data for temperature and voltage were recorded operating at a constant low current. Figure 40 shows the data of an ETP bar

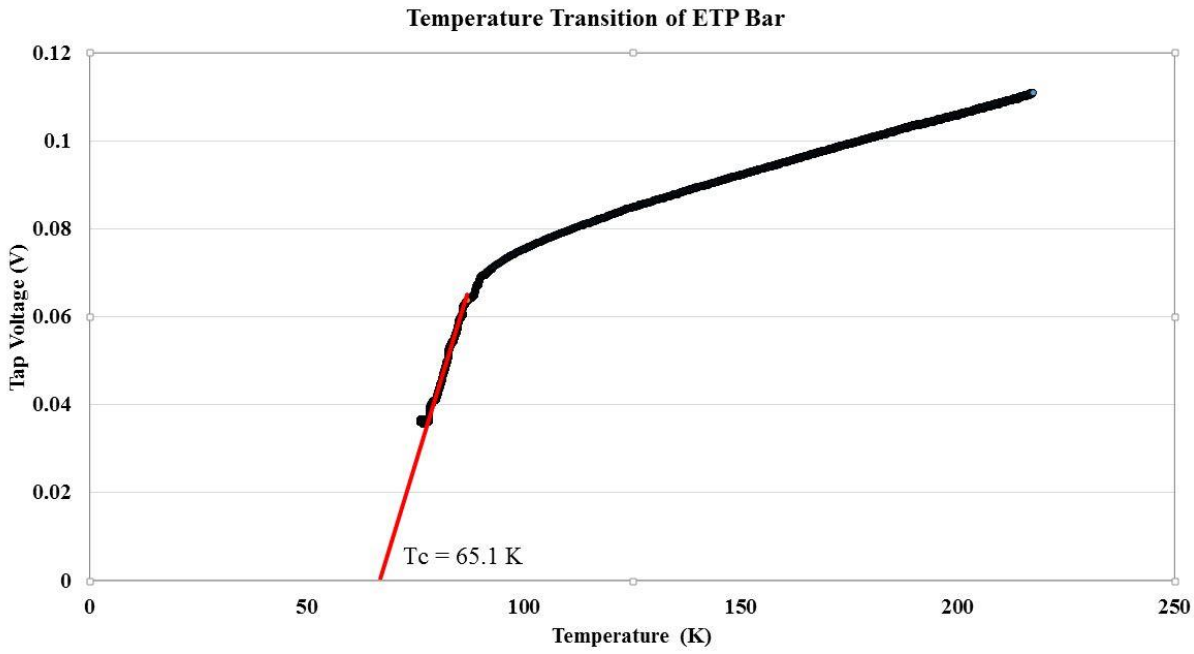

Figure 40: Data showing critical temperature of an ETP bar heat treated to a maximum temperature of 879 C.

*Part of the data reported in this section has been submitted for publication and reprinted from J N Kellams *et al* Presented at 2018 ICEC-ICMC, Oxford, England

that was heat treated to a maximum temperature of 879 C for 24 hours. The transition temperature of 65.1 K is even lower than that of the initial four point resistance test discussed in section 2. However, the transition has broadened indicating that the ETP bars are being doped non-homogenously, which is to be expected for such thick samples. It is clear that the material is in the middle of its transition at liquid nitrogen temperature. However, the material never reaches its full superconducting state allowing for true zero resistance. This data also tells us that the while the material does partially reach a mixed superconducting state, the typical gas environment of 1 atm of oxygen during heat treatment may not yield optimal results. Unfortunately, optimization for critical current at helium temperatures has no correlation to optimization of critical temperature.

6. ETP CURRENT TESTS AND RESULTS*

Current tests were performed on both ETP multifilament wires and ETP bars heat treated with maximum temperatures between 875.5 C and 879 at 0.5 C increments. None of the multifilament ETP wires displayed any superconductivity that could be detected. However, the ETP bars heat treated with a maximum temperature above 877.5 C showed clear superconductivity albeit with a significant residual resistance. This is undoubtedly due to the low transition temperature shown in section 5. The ETP bars heat treated below 877.5 C show no indication of superconductivity and clearly have a higher resistivity than the silver matrix of the

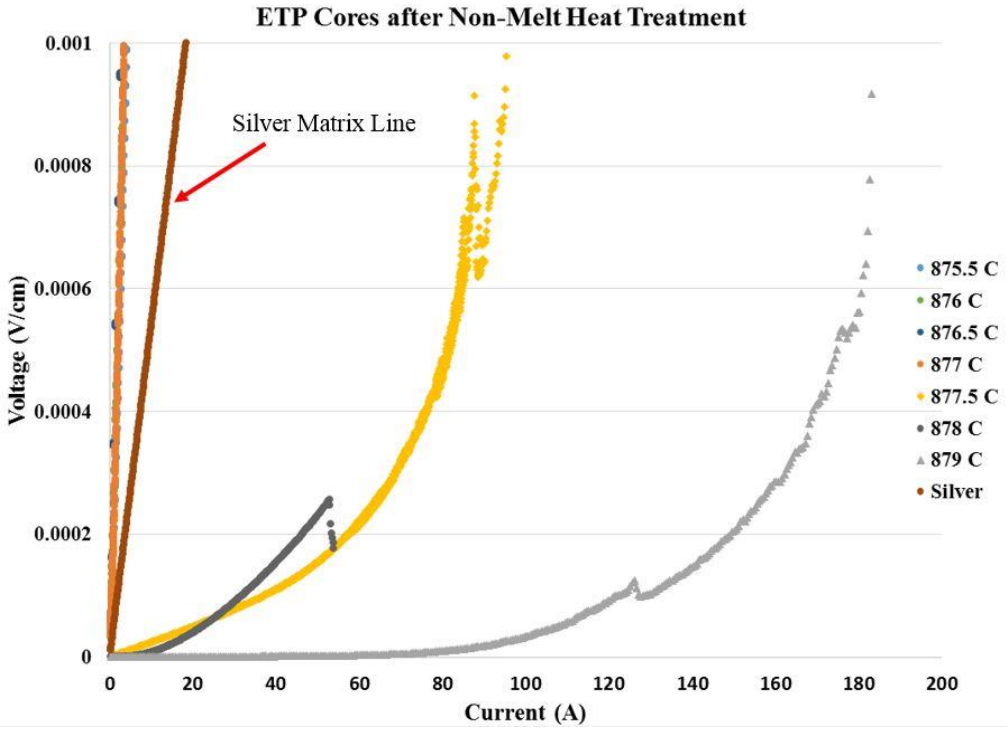

Figure 41: ETP bar current tests in liquid nitrogen, showing the bars that were heat treated to a maximum temperature of 877.5 C, 878 C, and 879 C all showed evidence of superconductivity.

*Part of the data reported in this section has been submitted for publication and reprinted from J N Kellams *et al* Presented at 2018 ICEC-ICMC, Oxford, England

wire. The data from the bars, shown in Figure 41, suggests that superconductivity would be seen in the wire samples heat treated alongside the ETP bars but this was not the case. The silver matrix line is included on the graph to illustrate that the resistivity of the ETP is higher than the silver matrix if it is not in a superconducting state. This explains why all of the multifilament wires tested only showed an ohmic line corresponding to the silver matrix.

Normally the criterion to define the critical current of a tested sample is the current at which the electric field exceeds 1 μV/cm. This criterion is only achieved for the ETP bars that were heat treated to a maximum temperature of 878 C and 879 C, albeit at the low currents of 5 A and 20 A respectively. Since the ETP bars from

Figure 42: ETP bars after heat treatment and current testing in liquid nitrogen. Notice the ETP bar with Tmax = 878.0 C broke during current testing.

the non-melt heat treatment have a very low critical temperature these results can not accurately determine a critical current in LN, but they can be used to verify that a superconducting transition is occurring for ETP bars that were heat treated using a non-melt heat profile.

Visual inspection of the bars, shown in Figure 42, proved that the bars did not melt. However, some of the bars do display softening of the edges and deformation.

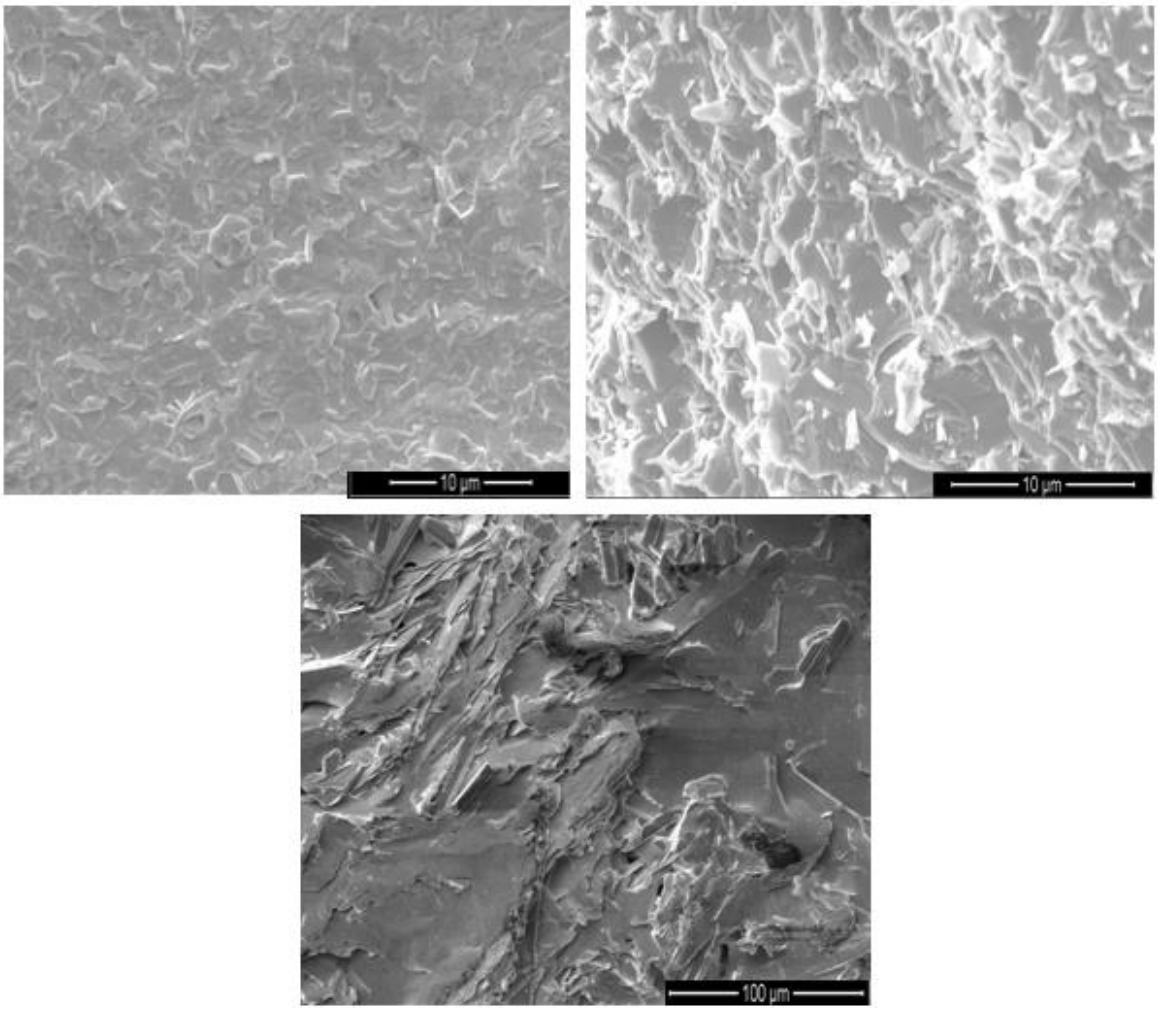

Figure 43: Micrographs of ETP bars heat treated to a maximum temperature of 879 C showing a (Top) portion of the bar with minimal deformation, (Middle) broken edge of ETP bar to view the internal texture of the bar, (Bottom) deformed area of the bar showing some loss of texture.

To verify beyond macroscopic visual inspection that the ETP bars did not melt and maintained the pre-texturing the samples were viewed under an SEM. The images, shown in Figure 43, clearly show that the samples did not melt. They all display clear grain growth and significant interconnectivity between grains. In addition, no parasitic phases were found as long as the sample was annealed. Texture was maintained internally for all samples viewed, but texture was reduced on the surface of the ETP bars heat treated at higher temperatures. This is believed to be due to the bars being unconstrained during heat treatment. It is clear that the bar did not melt, but softened especially for the samples treated very near to the melt point. The deformation was compounded by the bed of enhanced powder it sat on inside the silver boat during heat treatment.

7. CONCLUSIONS*

The methods developed in this work were successful in mixing nano-scale silver powder with ~ 1 micrometer scale phase pure Bi-2212 powder. The process developed by Kyle Damborsky [77] to uniaxially press Bi-2212 powder was significantly altered so the survival rate of the bars was drastically increased, while still producing the desired effects. The bars were then used to successfully fabricate multifilament wire up to 7 x 19 filaments. The wires that were made were on the order of ~15 meters, with no indications that scaling up to longer lengths would causes any issues.

The development of a non-melt heat treatment did successfully produce a superconductor but only for the bulk ETP bars, not for the multifilament wires. The ETP bars maintained the pre-texture and significant interconnectivity was seen in the SEM images. The strongest evidence of interconnectivity is the significant supercurrent that was carried. This is method is not on par with overpressure processing but it has been shown to be able to produce a viable textured superconductor without melting the bulk of the material. To make this method viable for use on wire, further process development will be necessary for the non-melt heat treatment. The entire heat schedule may need altered since melting of the bulk material is the basis for the standard heat treatment. This continued process development would need to be optimized for use in liquid helium as the end goal for this superconducting wire is use for high current application, not high temperature application. Unfortunately this further process development is beyond the scope of this dissertation and will have to be left to a future

*Part of the data reported in this section has been submitted for publication and reprinted from J N Kellams *et al* Presented at 2018 ICEC-ICMC, Oxford, England

generation of students. It is the opinion of the author that this further development is worthwhile but would require funding that was not available during this work.

REFERENCES

1. H. K. Onnes, in *KNAW* (Amsterdam, 1909), Vol. 11, pp. 168-185.

2. H. K. Onnes, in *KNAW* (Amsterdam, 1911), Vol. 13, pp. 1274-1276.

3. H. K. Onnes, in *KNAW* (Amsterdam, 1911), Vol. 14, pp. 113-115.

4. H. K. Onnes, in *KNAW* (Amsterdam, 1912), Vol. 14, pp. 818-821.

5. H. K. Onnes, in *KNAW* (Amsterdam, 1914), Vol. 16, pp. 673-688.

6. H. K. Onnes, in *KNAW* (Amsterdam, 1914), Vol. 17, pp. 12-20.

7. H. K. Onnes, in *KNAW* (Amsterdam, 1914), Vol. 17, pp. 278-283.

8. H. K. Onnes, in *KNAW* (Amsterdam, 1914), Vol. 17, pp. 514-519.

9. H. K. Onnes, in *KNAW* (Amsterdam, 1913), Vol. 15, pp. 1406-1430.

10. H. K. Onnes, in *KNAW* (Amsterdam, 1914), Vol. 17, pp. 520-527.

11. B. Beckman and H. K. Onnes, in *KNAW* (Amsterdam, 1912), Vol. 15, pp. 307-318.

12. B. Beckman and H. K. Onnes, in *KNAW* (Amsterdam, 1912), Vol. 15, pp. 319-321.

13. W. Meissner and R. Ochsenfeld, Naturwissenschaften **21**, 787-788 (1933).

14. F. London and H. London, in *Proceedings of the Royal Society A* (The Royal Society, 1935), Vol. 149.

15. *Meissner Effect*, < https://en.wikipedia.org/wiki/Meissner_effect> (2018).

16. L. V. Shubnikov, V. I. Khotkevich, Y. D. Shepelev and Y. N. Ryabinin, Zh Eksper. Teor. Fiz. **7**, 221-237 (1937).

17. V. L. Ginzburg and L. D. Landau, Zh. Eksp. Theor. Fiz. **20** (1950).

18. N. V. Zavaritski, Dokl. Akad. Nauk SSSR **86** (1952).

19. A. A. Abrikosov, Dokl. Akad. Nauk SSSR **86** (1952).

20. D. Cribier, B. Jacrot, L. Madhav Rao and B. Farnoux, Physics letters **9** (2), 106-107 (1964).

21. D. Cribier, B. Jacrot, L. Madhav Rao and B. Farnoux, in *Progress in Low Temperature Physics* (1967), Vol. 5, pp. 161-180.

22. U. Essmann and H. Trauble, Physics Letters **24A** (10), 526-527 (1967).

23. F. S. Wells, A. V. Pan, X. R. Wang, S. A. Fedoseev and H. Hilgenkamp, Sci Rep **5**, 8677 (2015).

24. G. Blatter, M. V. Feigel'man, V. B. Geshkenbein, A. I. Larkin and V. M. Vinokur, Reviews of Modern Physics **66** (4), 1125-1388 (1994).

25. M. Zehetmayer, Sci Rep **5**, 9244 (2015).

26. A. I. Larkin and Y. N. Ovchinnikov, Journal of Low Temperature Physics **34** (3/4), 409-428 (1979).

27. J. Bardeen, L. N. Cooper and J. R. Schrieffer, Physical Review **108** (5), 1175-1204 (1957).

28. D. C. Johnston, Advances in Physics **59** (6), 803-1061 (2010).

29. A. P. Drozdov, M. I. Eremets, I. A. Troyan, V. Ksenofontov and S. I. Shylin, (arxiv, 2015).

30. J. G. Bednorz and K. A. Muller, Z. Phys. B - Condensed Matter **64**, 189-193 (1986).

31. M. K. Wu, J. R. Ashburn, C. J. Torng, P. H. Hor, R. L. Meng, L. Gao, Z. J. Huang, Y. Q. Wang and C. W. Chu, Phys Rev Lett **58** (9), 908-910 (1987).

32. H. Maeda, Y. Tanaka, M. Fukutomi and T. Asano, Japanese Journal of Applied Physics **27** (2), L209-L210 (1988).

33. P. Monthoux, A. V. Balatsky and D. Pines, Physical Review B **46** (22), 14803-14817 (1992).

34. S. Chakravarty, A. Sudbo, P. W. Anderson and S. Strong, in *Science* (1993), Vol. 261, pp. 337-340.

35. D. J. Van Harlingen, Reviews of Modern Physics **67** (2), 515-535 (1995).

36. B. Keimer, S. A. Kivelson, M. R. Norman, S. Uchida and J. Zaanen, Nature **518** (7538), 179-186 (2015).

37. V. L. Ginzburg and L. D. Landau, Zh Eksper. Teor. Fiz. **23**, 236-238 (1952).

38. D. R. Tillery, Proceeding of the Physical Society **86**, 289-295 (1965).

39. W. R. Lawrence and S. Doniach, presented at the 12th International Conference on Low Temperature Physics, Kyoto, Japan, 1971 (unpublished).

40. R. A. Klemm, A. Luther and M. R. Beasley, Physical Review B **12** (3), 877-891 (1975).

41. S. N. Artemenko and A. N. Kruglov, Physics Letters A **143** (9), 485-488 (1990).

42. J. R. Clem, Physical Review B **43** (10), 7837-7846 (1991).

43. A. Buzdin and D. Feinberg, J. Phys. France **51** (17), 1971-1978 (1990).

44. A. Engel, PhD Thesis, Victoria University of Wellington, 2001.

45. K. Matsumoto, P. Mele, A. Ichinose, M. Mukaida, Y. Yoshida, S. Horii and R. Kita, IEEE Transactions on Applied Superconductivity **19** (3), 3248-3253 (2009).

46. P. H. Kes, J. Aarts, V. M. Vinokur and C. J. van der Beek, Phys Rev Lett **64** (9), 1063-1066 (1990).

47. *Handbook of Applied Superconductivity*. (Institute of Physics Publishing, Bristol and Philadelphia, 1998).

48. Y. Terao, M. Sekino and H. Ohsaki, IEEE Transactions on Applied Superconductivity **22** (3), 5201904-5201904 (2012).

49. W. Buckles and W. V. Hassenzahl, IEEE Power Engineering Review **20** (5), 16-20 (2000).

50. T. Ichihara, K. Matsunaga, M. Kita, I. Hirabayashi, M. Isono, M. Hirose, K. Yoshii, K. Kurihara, O. Saito, S. Saito, M. Murakami, H. Takabayashi, M. Natsumeda and N. Koshizuka, IEEE Transactions on Appiled Superconductivity **15** (2), 2245-2248 (2005).

51. D. C. Larbalestier, A. Gurevich, D. M. Feldmann and A. Polyanskii, in *Nature* (Macmillan Magazines, 2001), Vol. 414.

52. M. Ono, S. Koga and H. Ohtsuki, IEEE Instrumentation & Measurement Magazine **5** (1), 9-15 (2002).

53. T. C. Cosmus and M. Parizh, IEEE Transactions on Applied Superconductivity **21** (3), 2104-2109 (2011).

54. E. Todesco and P. Ferracin, IEEE Transactions on Appiled Superconductivity **22** (2012).

55. L. Rossi, A. Badel, M. Bajko, A. Ballarino, L. Bottura, M. M. J. Dhalle, M. Durante, P. Fazilleau, J. Fleiter, W. Goldacker, E. Haro, A. Kario, G. Kirby, C. Lorin, J. van Nugteren, G. de Rijk, T. Salmi, C. Senatore, A. Stenvall, P. Tixador, A. Usoskin, G. Volpini, Y. Yang and N. Zangenberg, IEEE Transactions on Applied Superconductivity **25** (3), 1-7 (2015).

56. T. G. Berlincourt and R. R. Hake, Bull. Am Phys. Soc. **7** (1962).

57. R. Q. Apsey, D. E. Baynham, P. T. M. Clee, D. Cragg, N. Cunliffe, R. B. Hopes and R. V. Stovold, IEEE Transactions on Magnetics **MAG-21** (2), 490-493 (1985).

58. L. Bottura and A. Godeke, in *Reviews of Accelerator Science and Technology* (2013), pp. 25-50.

59. *Conectus*, <https://conectus.org/market/> (2018).

60. Z. Charifoulline, IEEE Transactions on Applied Superconductivity **16** (2), 1188-1191 (2006).

61. B. T. Matthias, T. H. Geballe, S. Geller and E. Corenzwit, Physical Review **95** (6), 1435-1435 (1954).

62. A. M. Clogston, Physical Review Letters **9** (6), 266-267 (1962).

63. J. J. Hanak, K. Strater and G. W. Cullen, RCA Review **25**, 342-365 (1964).

64. K. Zhang, P. Zhang, J. Guo, J. Jia, Y. Shi, J. Liu, H. Gao, J. Li, X. Liu and Y. Feng, IEEE Transactions on Applied Superconductivity **26** (3), 1-4 (2016).

65. B. Jakob and G. Pasztor, IEEE Transactions on Magnetics **32** (4), 2886-2889 (1996).

66. C. V. Renaud, in *AIP Conference Proceedings* (2004), pp. 376-381.

67. S. Caspi and P. Ferracin, presented at the Particle Accelerator Conference, Knoxville, Tennessee, 2005 (unpublished).

68. M. Solovyov, E. Pardo, J. Šouc, F. Gömöry, M. Skarba, P. Konopka, M. Pekarčíková and J. Janovec, Superconductor Science and Technology **26** (11) (2013).

69. J. D. Weiss, T. Mulder, H. J. ten Kate and D. C. van der Laan, Superconductor Science and Technology **30** (1) (2017).

70. P. C. Michael, L. Bromberg, D. C. van der Laan, P. Noyes and H. W. Weijers, Superconductor Science and Technology **29** (4) (2016).

71. D. D. Gulamova, D. E. Uskenbaev, D. G. Chigvinadze and O. V. Magradze, Applied Solar Energy **44** (1), 42-45 (2008).

72. A. I. Golovashkin, O. M. Ivanenko, Y. B. Kudasov, K. V. Mitsen, A. I. Pavlovsky, V. V. Platonov and O. M. Tatsenko, Physica C: Superconductivity **185-189**, 1859-1860 (1991).

73. X. H. Chen, M. Yu, K. Q. Ruan, S. Y. Li, Z. Gui, G. C. Zhang and L. Z. Cao, Physical Review B **58** (21), 14219-14222 (1998).

74. X. Xiang, W. A. Vareka, A. Zettl, J. L. Corkill, M. L. Cohen, N. Kijima and R. Gronsky, Phys Rev Lett **68** (4), 530-533 (1992).

75. A. Pomar, M. V. Ramallo, J. Mosqueira, C. Torron and F. Vidal, Physical Review B **54** (10) (1996).

76. *Bismuth Strontium Calcium Copper Oxide*, <https://en.wikipedia.org/wiki/Bismuth_strontium_calcium_copper_oxide> (2018).

77. K. C. Damborsky, PhD Dissertation, Texas A&M University, 2014.

78. F. Kametani, J. Jiang, M. Matras, D. Abraimov, E. E. Hellstrom and D. C. Larbalestier, Sci Rep **5**, 8285 (2015).

79. T. Lang, B. Heeb, D. Buhl and L. J. Gauckler, presented at the Fourth International Conference and Exhibition: World Congress on Superconductivity, Orlando, Florida, 1994 (unpublished).

80. Q. B. Hao, C. S. Li, S. N. Zhang, G. S. Li, L. F. Bai, G. Q. Liu and P. X. Zhang, Materials Science Forum **745-746**, 168-172 (2013).

81. D. C. Larbalestier, J. Jiang, U. P. Trociewitz, F. Kametani, C. Scheuerlein, M. Dalban-Canassy, M. Matras, P. Chen, N. C. Craig, P. J. Lee and E. E. Hellstrom, Nat Mater **13** (4), 375-381 (2014).

82. P. Majewski, R. Nast and F. Aldinger, Superconductor Science and Technology **12**, 249-254 (1999).

83. J. Jiang, W. L. Starch, M. Hannion, F. Kametani, U. P. Trociewitz, E. E. Hellstrom and D. C. Larbalestier, Superconductor Science and Technology **24** (8) (2011).

84. H. Miao, K. R. Marken, M. Meinesz, B. Czabaj and S. Hong, IEEE Transactions on Appiled Superconductivity **15** (2), 2554-2557 (2005).

85. K. Zhang, H. Higley, L. Ye, S. Gourlay, S. Prestemon, T. Shen, E. Bosque, C. L. English, J. Y. Jiang, Y. Kim, J. Lu, U. P. Trociewitz, E. E. Hellstrom and D. C. Larbalestier, Superconductor Science and Technology (2018).

86. J.-G. Qin, Y. Wu, J.-G. Li, C. Dai, F. Liu, H.-J. Liu, P.-H. Liu, C.-S. Li, Q.-B. Hao, C. Zhou and S. Liu, IEEE Transactions on Applied Superconductivity **27** (4), 1-5 (2017).

87. H.-j. Liu, H.-j. Ma, F. Liu, Y. Shi, J.-g. Qin, Y. Wu, J.-g. Li and L. Lei, IEEE Transactions on Applied Superconductivity **28** (4), 1-4 (2018).

88. C. Scheuerlein, M. Di Michiel, M. Scheel, J. Jiang, F. Kametani, A. Malagoli, E. E. Hellstrom and D. C. Larbalestier, Superconductor Science and Technology **24** (11) (2011).

89. J. Kadar, C. Scheuerlein, M. O. Rikel, M. Di Michiel and Y. Huang, Superconductor Science and Technology **29** (10) (2016).

90. T. Hasegawa, H. Kobayashi, H. Kumakura, H. Kitaguchi and K. Togano, Physica C: Superconductivity **222**, 118 (1994).

91. J. S. Luo, N. Merchant, V. A. Maroni, G. N. Riley and W. L. Carter, Applied Physics Letters **63** (5), 690-692 (1993).

92. F. Kametani, T. Shen, J. Jiang, C. Scheuerlein, A. Malagoli, M. Di Michiel, Y. Huang, H. Miao, J. A. Parrell, E. E. Hellstrom and D. C. Larbalestier, Superconductor Science and Technology **24** (7) (2011).

93. E. E. Hellstrom and W. Zhang, Superconductor Science and Technology **8**, 317-323 (1995).

94. T. Hasegawa, N. Ohtani, T. Koizumi, Y. Aoki, S. Nagaya, N. Hirano, L. Motowidlo, R. S. Sokolowski, R. M. Scanlan, D. R. Dietderich and S. Hanai, IEEE Transactions on Appiled Superconductivity **11** (2001).

95. H. Miao, Y. Huang, S. Hong, M. Gerace and J. Parrell, Journal of Physics: Conference Series **507** (2) (2014).

96. J. L. Reeves, M. Polak, W. Zhang, E. E. Hellstrom, S. E. Babcock, D. C. Larbalestier, N. Inoue and M. Okada, IEEE Transactions on Appiled Superconductivity **7** (2), 1541-1543 (1997).

97. A. Malagoli, C. Bernini, V. Braccini, G. Romano, M. Putti, X. Chaud and F. Debray, (arXiv, 2013).

98. T. Lang, D. Buhl and L. J. Gauckler, Superconductor Science and Technology **10** (1997).

99. P. Majewski, A. Aubele and F. Aldinger, Physica C: Superconductivity **341-348**, 517-518 (2000).

100. S. T. Misture, D. P. Matheis, R. L. Snyder, T. N. Blanton, G. M. Zorn and B. Seebacher, Physica C: Superconductivity **250**, 175-183 (1995).

101. J. N. Kellams, K. Damborsky, P. M. McIntyre, J. Vandergrifft, L. Motowidlo and N. Pogue, presented at the International Particle Accelerator Conference, Richmond, VA, 2015 (unpublished).

102. J. Kellams, in *IOP Conference Series: Materials Science and Engineering* (Tuscon, AZ, 2015), Vol. 102.

103. M. N. Rahaman, *Ceramics Processing*. (CRC Press, Boca Raton, FL, 2007).

104. S. M. Khalil and A. Sedky, Physica B: Condensed Matter **357** (3-4), 299-304 (2005).

105. L. Motowidlo, (private communication).

106. Z. Konstantinovic, Z. Z. Li and H. Raffy, Physica B **259-261**, 567-568 (1999).

APPENDIX A

This appendix is the step by step checklist that was used when making ETP bars. It was written to be used by the author of this work, and the students that were helping with the project. This begins with the assumption that the parts of the just finished being used to make an ETP bar, and that bar was removed. All cleaning and Bi-2212 work should be done on the down draft table, with proper PPE for powder handling.

ETP bar fabrication Procedure

_____ Disassemble the inner portions of the die completely, removing bolts, die pieces, shims, and the hammer assembly. Leave the out ring of the die secured.

_____ Use the spatula to scrape excess 2212 off of surfaces that may be stuck from the pressing process.

_____ Clean all of the parts thoroughly with acetone and Kimwipes to remove as much powder as possible, note that all of the Bi-2212 pressed powder may not come off in this step.

_____ Clean all parts with ethyl alcohol and Kimwipes to remove acetone residue.

_____ Preheat oven to about 80 degrees C

_____ Put all parts, including die pieces, hammer assembly pieces, and tools in the glass jar with Alcanox detergent and RO water, in the sonic cleaner to break up and deposits that could not be removed above. Let this sit for about 1-2 hours or so until the 2212 is completely removed from the surfaces. (Alcanox and RO water should be changed every few times)

_____ Take pieces out of sonic cleaner and rinse with RO water to remove detergent. The parts may need to be rinsed for up to a minute each depending on the amount of detergent used.

_____ Swish pieces in the jar of ethyl alcohol to remove water, and place in the 80 degree C oven.

_____ While the parts are in the supersonic cleaner and drying in the oven, use this time to thoroughly clean the rest of the die (outer ring, base and top) with acetone and then ethyl alcohol if necessary. Be sure to remove any 2212 powder that may have spilled during the fill, or had been pushed out during the pressing process.

_____ Clean the powder slide using ethyl alcohol ONLY! Acetone with dissolve the epoxy holding it together.

_____ Put double sided tape on both top and bottom die assemblies, to be used when attaching the nitrogen tent.

_____ Cut (152mm x 35mm) blued stainless steel shims (0.002 inch thick), leaving the bottom edge of the shim uncut, with the paper cutter and clean stainless steel shims using acetone, then ethyl alcohol, being sure to leave minimal residue behind.

_____ When all the parts are all completely dry, turn the oven off and allow them to cool.

_____ Inspect all of the parts for alcohol residue and try to wipe it off when necessary.

_____ Assemble both the die and hammer assembly, being sure to place the shims in between the walls of the die and the bottom piece. Use the tamping bar to do

this, clip shims to the tamping bar flush with the top so that some of the shim is in between the side and bottom of the die. Be sure that the uncut edge of the shims is facing into the die.

_____ Carefully fill the gap with 9.3 grams of 2212 powder using the slide, taking care to not spill or overflow the gap. It is very important to get the powder as uniform as possible. You will need to gently and uniformly press some of the powder down with the tamping bar after about half of the powder has been filled.

_____ Once the slot is filled and uniform distribution is achieved, push the hammer of the die into the slot with the curved side down. Be care to do your best to have it straight as it is a very tight fit.

_____ Put the hammer assembly into the press and attach it to the top via bolts and spacers.

_____ Put the die assembly into the press, and align it with the hammer assembly.

_____ Raise the die assembly taking care that the die is fully aligned with the hammer. (The bearing sheathes should slide easily in and out of the die assembly). Also the shims may need to be spread slightly to make sure the hammer goes in between the two shims. The shims should be spread VERY CAREFULLY using the spatulas (May require two people). If the shims are flicked or bent and let go suddenly then powder can go everywhere.

_____ Seal the entire die assembly in the plastic tent, purge the air in the tent with argon tent and then have about 2-3 cubic feet per hour flowing into the tent for the duration of the pressing procedure.

_____ Zero the pressure gauge

_____ SLOWLY (close off the valve most of the way) press the powder to 20 KSI at the powder, this is 271 psi at the press using 6 cylinders. I find it best to use the hand pump for the last 50 or so psi.

_____ Allow the press to relax and pump the press back up to keep the pressure at 271 psi on the gauge. This can take quite some time 30-60 mins. I generally stop when the pressure only drops by about one psi per minute.

_____ Lower the press slowly being sure that the die and the hammer assemblies separate.

_____ Carefully remove the die and hammer assemblies, and cart them to the down draft table.

_____ VERY CAREFULLY remove the inner die piece (two of them), and VERY CAREFULLY remove the pressed 2212 bar. The bars are very fragile and do not respond well to shear forces or mechanical shock.

_____ Make sure the bar is straight.

_____ Place the ETP bar into the glove box using proper procedure.

_____ If the ETP bar needs shortened, score the 2212 bar at the desired length using a razor blade, and once scored enough break at the score. It is best to avoid this if possible as this is one of the most likely times a bar will break in an unwanted way.

_____ Use the file to flatten the ends, and shave the long edges using the fixture in the glove box. Be very careful when handling the bars during this step. This is the most likely time that a bar will break.

_____ Carefully slide the shaved bar into the silver tube with the correct alignment

_____ Record all pertinent information immediately.